

DTIC FILE COPY

2

NAVAL POSTGRADUATE SCHOOL
Monterey, California

AD-A219 841



THESIS

DTIC
ELECTE
MAR 29 1990
S E D

A CORRELATION STUDY OF WIND SPEED
AS MEASURED BY THE
SPECIAL SENSOR: MICROWAVE/IMAGER
AND THE GEOSAT ALTIMETER

by

James E. Lilly

September 1989

Co-Advisor:
Co-Advisor:

Jeffery A. Nystuen
Andreas K. Goroch

Approved for public release; distribution is unlimited

90 03

REPORT DOCUMENTATION PAGE

1a. REPORT SECURITY CLASSIFICATION UNCLASSIFIED			1b. RESTRICTIVE MARKINGS		
2a. SECURITY CLASSIFICATION AUTHORITY			3. DISTRIBUTION/AVAILABILITY OF REPORT Distribution is unlimited		
2b. DECLASSIFICATION/DOWNGRADING SCHEDULE					
4. PERFORMING ORGANIZATION REPORT NUMBER(S)			5. MONITORING ORGANIZATION REPORT NUMBER(S)		
6a. NAME OF PERFORMING ORGANIZATION Naval Postgraduate School		6b. OFFICE SYMBOL (if applicable) 35	7a. NAME OF MONITORING ORGANIZATION Naval Postgraduate School		
6c. ADDRESS (City, State, and ZIP Code) Monterey, CA 93943-5000			7b. ADDRESS (City, State, and ZIP Code) Monterey, CA 93943-5000		
8a. NAME OF FUNDING/SPONSORING ORGANIZATION		8b. OFFICE SYMBOL (if applicable)	9. PROCUREMENT INSTRUMENT IDENTIFICATION NUMBER		
8c. ADDRESS (City, State, and ZIP Code)			10. SOURCE OF FUNDING NUMBERS		
			Program Element No	Project No	Task No
			Work Unit Accession Number		
11. TITLE (Include Security Classification) A CORRELATION STUDY OF WIND SPEED AS MEASURED BY THE SPECIAL SENSOR MICROWAVE IMAGER AND THE GEOSAT ALTIMETER					
12. PERSONAL AUTHOR(S) Lilly, James, E.					
13a. TYPE OF REPORT Master's Thesis		13b. TIME COVERED From To		14. DATE OF REPORT (year, month, day) September 1989	
				15. PAGE COUNT 79	
16. SUPPLEMENTARY NOTATION The views expressed in this thesis are those of the author and do not reflect the official policy or position of the Department of Defense or the U.S. Government					
17. COSATI CODES			18. SUBJECT TERMS (continue on reverse if necessary and identify by block number)		
FIELD	GROUP	SUBGROUP	SSM/I, GEOSAT, remote sensing, wind speed		
19. ABSTRACT (continue on reverse if necessary and identify by block number) Wind speed data is routinely acquired at the FLEET NUMERICAL OCEANOGRAPHIC CENTER (FNOC) in near real time from the SPECIAL SENSOR MICROWAVE IMAGER, on board the DEFENSE METEOROLOGICAL SATELLITE (DMSP) satellite and the RADAR ALTIMETER on board the GEOSAT satellite. A correlation study is made of the SSM/I and ALTIMETER wind speed data using five data sets from areas where the DMSP satellite had crossed within 1.1 hours of the GEOSAT satellite. Regions of ocean where the atmosphere was free of cloud water and precipitation have a high correlation of approximately 0.995, while areas with precipitation and cloud water have a very poor correlation. Areas of high water vapor content do not appear to adversely affect the high correlation between the SSM/I and ALTIMETER measured wind speeds.					
20. DISTRIBUTION/AVAILABILITY OF ABSTRACT <input checked="" type="checkbox"/> UNCLASSIFIED-UNLIMITED <input type="checkbox"/> SAME AS REPORT <input type="checkbox"/> DTIC USERS			21. ABSTRACT SECURITY CLASSIFICATION Unclassified		
22a. NAME OF RESPONSIBLE INDIVIDUAL Jeffery A. Nystuen			22b. TELEPHONE (Include Area code) 1-408-646-2917		22c. OFFICE SYMBOL 68NY

DD FORM 1473, 84 MAR

83 APR edition may be used until exhausted
All other editions are obsoleteSECURITY CLASSIFICATION OF THIS PAGE
Unclassified

Approved for public release; distribution is unlimited.

A Correlation Study of Wind Speed
as Measured by the
Special Sensor Microwave Imager
and the Geosat Altimeter

by

James E. Lilly
Lieutenant, United States Navy
B.S., University of South Carolina

Submitted in partial fulfillment
of the requirements for the degree of

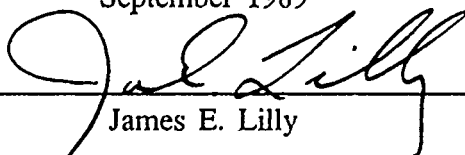
MASTER OF SCIENCE IN METEOROLOGY AND PHYSICAL OCEANOGRAPHY

from the

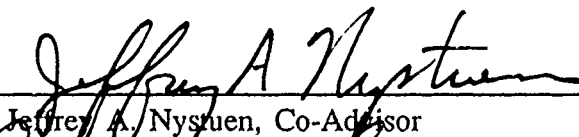
NAVAL POSTGRADUATE SCHOOL

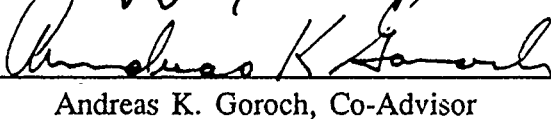
September 1989

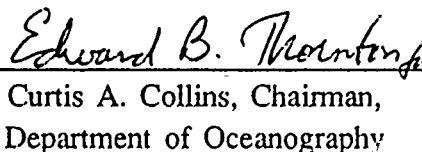
Author:


James E. Lilly

Advised by:


Jeffrey A. Nystuen, Co-Advisor


Andreas K. Goroch, Co-Advisor


Curtis A. Collins, Chairman,
Department of Oceanography

ABSTRACT

Wind speed data is routinely acquired at the FLEET NUMERICAL OCEANOGRAPHIC CENTER (FNOC) in near real time from the SPECIAL SENSOR MICROWAVE/IMAGER (SSM/I), on board the DEFENSE METEOROLOGICAL SATELLITE PROGRAM (DMSP) satellite and the RADAR ALTIMETER on board the GEOSAT satellite. A correlation study is made of the SSM/I and ALTIMETER wind speed data using five data sets from areas where the DMSP satellite had crossed within 1.1 hours of the GEOSAT satellite. Regions of ocean where the atmosphere was free of cloud water and precipitation have a high correlation of approximately 0.995, while areas with precipitation and cloud water have very poor correlation. Areas of high water vapor content do not appear to adversely affect the high correlation between the SSM/I and ALTIMETER measured wind speeds.

*Keynote for Marine meteorology
Meteorological satellite data, primary/satellite
Atmospheric pressure, temperature, humidity, Remote sensing
Threats. (EDC) **

Accession For	
NTIS GRA&I	<input checked="" type="checkbox"/>
DTIC TAB	<input type="checkbox"/>
Unannounced	<input type="checkbox"/>
Justification	
By	
Distribution/	
Availability Codes	
Dist	Avail and/or Special
A-1	



TABLE OF CONTENTS

I. INTRODUCTION	1
II. FUNDAMENTALS OF MICROWAVE REMOTE SENSING	4
A. PROPERTIES OF EM WAVE PROPAGATION AND ATTENUATION	4
B. POLARIZATION	8
C. BRIGHTNESS TEMPERATURE	10
D. ABSORPTION AND SCATTERING OF RADIATION	13
E. THE RELATION OF SURFACE ROUGHNESS TO EMITTED RADIATION	13
F. THE RADIATIVE TRANSFER EQUATION	15
G. THE TRANSFER OF MOMENTUM FROM THE ATMOSPHERIC SURFACE LAYER TO THE SEA SURFACE	16
III. MEASURING WIND SPEED OVER THE OCEAN WITH THE SSM/I ...	20
IV. MEASURING WIND SPEED OVER THE OCEAN WITH THE GEOSAT ALTIMETER	23
V. GROUND TRUTH STUDIES	26

A.	GEOSAT Wind Speed Ground Truth Study	26
B.	SSM/I WIND SPEED GROUND TRUTH STUDY	28
VI.	SSM/I AND GEOSAT ALTIMETER WIND SPEED COMPARISON	30
A.	DATA ACQUISITION	30
B.	DATA FORMATS AND PROCESSING	31
1.	SSM/I Data Base	31
2.	GEOSAT Data Base	32
3.	Processing GEOSAT Altimeter and SSM/I data sets	33
C.	DATA ANALYSIS AND RESULTS	33
1.	Orbit 9138, 27 March, 1989	35
2.	Orbit 8934, 13 March, 1989	36
3.	Orbit 8058(7), 10 January, 1989	40
4.	Orbit 8058(6), 10 January, 1989	51
5.	Orbit 7925, 2 January, 1989	56
VII.	CONCLUSIONS	64
	LIST OF REFERENCES	68
	INITIAL DISTRIBUTION LIST	70

I. INTRODUCTION

Understanding the environment has been a problem mankind has dealt with for ages. Our knowledge of the earth was initially limited to that which we could see with our own eyes. Gradually our ability to sense our environment grew as new instruments were developed. When space satellites came onto the scene, a rich resource of information concerning the world around us suddenly opened. From visual and infrared images of the earth, the truly dynamic nature of the planet we live on could finally be appreciated.

The years following the first attempts at retrieving environmental data from space have shown advances that parallel those made in computer technology. Devices have been implemented which have made use of virtually all of the electromagnetic (EM) spectrum. Each remote sensing device was designed for the purpose of detecting some form of radiation either emitted or reflected by the earth. To observe particular features of the atmosphere or ocean, methods were developed which would utilize particular frequencies to penetrate through obstacles in the path of this radiation and arrive at its target parameter.

Wind speed over the ocean has proven to be a particularly difficult parameter to measure, but most worthwhile to pursue. Vast areas of ocean have been "data deserts" for years. Remote sensing of these regions using microwave frequencies can supply data to improve "data starved" numerical input for environmental models. This, in turn, should offer a better understanding of synoptic weather systems, improving on the visible and infrared technologies currently used today. Disseminating

information concerning the global surface wind field to all vessels, would enhance preparations for oceanic transit. Ships already underway would be better prepared for heavy winds and seas.

In the case of wind speed over the ocean, two separate techniques have been developed. The first is the active radar device known as the GEOSAT altimeter which utilizes pulses of EM energy at 13.7 GHz to analyze the surface of the ocean. Though its prime objective was to map the earth's geoid, its signal can also be used to measure surface wave height and wind speed over the ocean. The second device known as the SPECIAL SENSOR MICROWAVE IMAGER (SSM/I) utilizes a totally different approach to the problem of wind speed measurement. Instead of transmitting its own radiation to the earth and then receiving a returned signal for analysis, it passively measures upwelling radiation from the earth's atmosphere and oceans.

How these two methodologies compare, is the subject of this thesis. The data utilized in this comparison represents several areas of the world where both satellites were co-located within one hour of each other's orbit. In the pages to follow, details of how each system operates and the physics behind the analysis of the data, will be explored. Correlation studies made for each region will disclose similarities and differences in the wind speed measurements. A particularly interesting case will be presented where several environmental parameters have interfered with the sensors ability to accurately access the surface wind speed.

Chapter two details the basic physics applicable to the SSM/I and GEOSAT remote sensors, as well as the operation of both systems. Chapter three will discuss ground truth verification studies made for each system. Here, individual strengths and

weaknesses are taken into account prior to the comparison study. The experiment is presented in chapter four, followed by conclusions and recommendations in chapter five.

II. FUNDAMENTALS OF MICROWAVE REMOTE SENSING

The basic physics behind the remote sensing techniques examined in this thesis, will be discussed in this chapter. The first section will cover the propagation characteristics of EM radiation. This will be followed by an overview of the index of refraction, blackbody radiation, emissivity, and the radiative-transfer equation. This should provide an ample background for understanding the operation of both the SSM/I and the GEOSAT altimeter.

A. PROPERTIES OF EM WAVE PROPAGATION AND ATTENUATION

Microwave remote sensing depends on the modification of EM radiation by the environment. Changes take place in the phase and intensity of an EM wave as it passes through the atmosphere and interacts with the ocean surface. These alterations of the wave's character are interpreted by the remote sensing device as variations in the state of the environment. We will first describe the EM wave equation and then develop the relationships that govern the changes that take place in the wave as it passes through matter.

EM radiation consists of alternating electric and magnetic fields [Ref. 1], which are classified by their frequency of fluctuation. A single EM wave vector, $E(x,y,z)$, can be broken down into its individual components, E_x , E_y , and E_z for a simplified analysis (Fig.1). The propagation characteristics of a single component of an EM wave

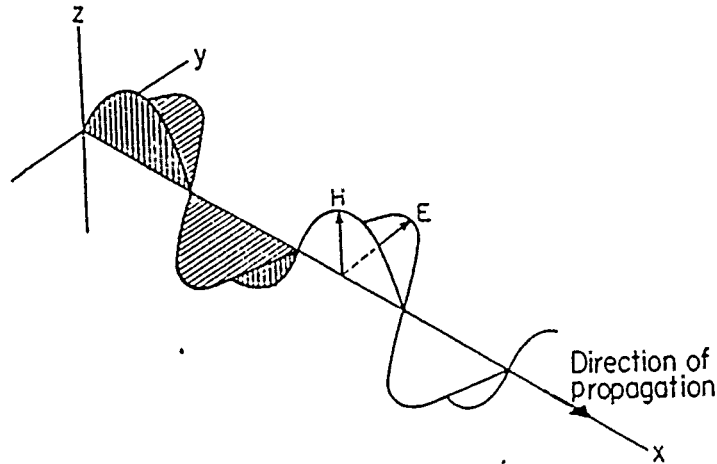


Figure 1 Electromagnetic wave vector and components.

can be described by the following equations:

$$E_y = E_0 e^{[-i(kx - \omega t)]} \quad (1)$$

$$k^2 = \omega^2 \mu \epsilon - i\omega \mu \quad (2)$$

$$\omega = 2\pi f \quad (3)$$

$$\mu = \mu_0 \mu_r \quad (4)$$

$$\epsilon = \epsilon_0 \epsilon_r = \epsilon_0 (\epsilon' - i\epsilon'') \quad (5)$$

where:

$E_y \equiv$ component of the electric field intensity

$E_0 \equiv$ initial electric field magnitude

$k \equiv$ complex wave number

$\omega \equiv$ frequency in radians per second

$f \equiv$ frequency in hertz

$\mu_o \equiv$ permeability of free space ($4\pi \times 10^{-7} \text{Hz/m}$)

$\mu_r \equiv$ relative permeability of a material (≈ 1)

$\epsilon \equiv$ permittivity of a medium

$\epsilon_o \equiv$ permittivity of free space ($8.85 \times 10^{-12} \text{ Farads/m}$)

$\epsilon', \epsilon'' \equiv$ real and imaginary components of the dielectric constant

For most cases in remote sensing applications, the value of $\mu_r = 1$, so that equation (2) can be written as:

$$k^2 = \omega^2 \mu_o \epsilon_o [\epsilon' - i\sigma/(\epsilon_o \omega)] \quad (6)$$

where:

$\epsilon_r = [\epsilon' - i\sigma/(\epsilon_o \omega)]$ the complex dielectric constant

$\sigma \equiv$ conductivity of the medium

In free space, i.e., a vacuum, $\epsilon_r = 1$, $\sigma = 0$, and the EM wave velocity is given as:

$$c_o^2 = 1/(\mu_o \epsilon_o) \quad (7)$$

For EM waves traveling through matter, such as the ocean or atmosphere, the velocity is determined through the equation:

$$c = \omega/k = c_o/\sqrt{\epsilon_r} \quad (8)$$

From (7) and (8), we can define the index of refraction n , which is related to ϵ_r by the formula:

$$n = c_o/c = \sqrt{\epsilon_r} \quad (9)$$

Equation (9) is important for understanding how the EM wave is effected as it passes through the atmosphere and interacts with the ocean below. Since n is related to the complex dielectric constant ϵ_r , radiation passing through matter will experience a

modification in speed and intensity. The wave will be slowed due to the resistance encountered by an induced electric field produced in this medium and attenuated through the imaginary component of n . To understand how the imaginary component can attenuate the wave, n must be examined in more detail. The index of refraction written in its component form:

$$n = \alpha + i\beta \quad (10)$$

where α and β represent the real and imaginary parts of n and are written as:

$$\alpha^2 = (|\epsilon_r| + \epsilon')/2 \quad (11)$$

$$\beta^2 = (|\epsilon_r| - \epsilon')/2 \quad (12)$$

$$|\epsilon_r| = [\epsilon'^2 + \sigma^2/(\epsilon_0\omega)^2]^{1/2} \quad (13)$$

Returning to equation (8) for the wave number k and substituting the component form of n into that expression, we can rewrite k as:

$$k = \omega\alpha/c + i\omega\beta/c \quad (14)$$

By replacing the expression for k in equation (14) into the original expression for the propagating wave, equation (1), we have:

$$\begin{aligned} E_y &= E_0 e^{[-i(\omega\alpha\beta/c - \omega t)]} e^{[\omega\beta x/c]} \\ &= E_0 e^{[\phi x]} e^{[-i(\omega\alpha x/c - \omega t)]} \end{aligned} \quad (15)$$

where $\phi = -\omega/c$ is known as the attenuation coefficient. With a negative value in the exponential, this component acts to reduce the value of the electric field as the EM wave passes through matter. The distance the radiation travels through some medium, in which the intensity of the wave is reduced by a factor of $\exp(-1)$, is known as the skin depth d and is given by :

$$d = c/(\omega\beta) \quad \text{or} \quad d = c/(2\pi f\beta) \quad (16)$$

For a frequency of 5 GHz, the value of d is 0.5 centimeters. The SSM/I operates between 19 and 37 GHz and the GEOSAT altimeter operates at 13.5 GHz, and so the skin depths for the instruments in this study are on the order of millimeters.

B. POLARIZATION

In addition to the variation of the intensity and frequency of the wave, microwave radiation is also characterized by its polarization. Polarization is defined as the orientation of the electric field vector relative to the surface it is reflected or emitted [Ref. 2]. Polarized radiation is classified as either horizontal, in which case the field is parallel to the surface, or vertical, whereby the field is perpendicular with respect to the surface. A change in surface conditions and viewing angle, will affect the vertically and horizontally polarized EM waves in different ways. The amount of radiation emitted from a surface (emissivity) depends on how the radiation is polarized (Fig.2). The SSM/I's sensors can detect both horizontally and vertically polarized radiation. Certain combinations of polarized frequencies are used to allow particular environmental parameters to be measured separately with a minimal of interference from the other parameters.

Assuming a smooth (specular) surface, the reflection of the spectral radiance, R , from such a surface is written in equation form as:

$$R(\lambda; \theta, \phi, -\pi) = L_r(\lambda; \theta, \phi) / L_i(\lambda; \theta, \phi, -\pi) \quad (17)$$

where:

$\lambda \equiv$ wavelength of the radiation

$\theta, \phi \equiv$ spherical coordinate angles

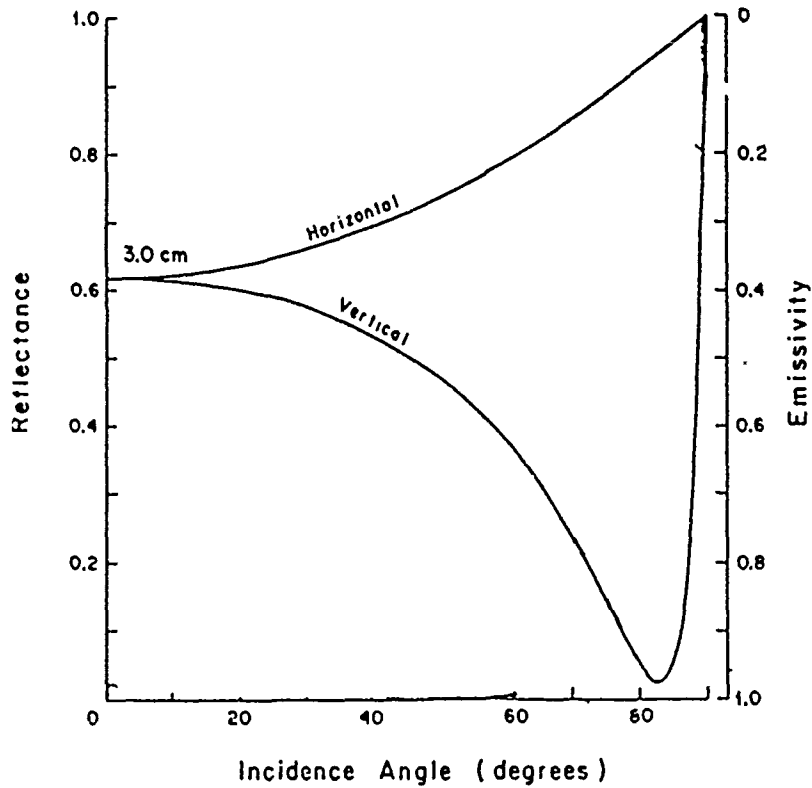


Figure 2 Polarized microwave radiation at 3 cm wavelength as a function of emissivity and incidence angle.

$L_r, L_i \equiv$ reflected and incident radiance respectively

The spectral reflectance of a plane dielectric surface is determined through the Fresnel reflection coefficients as follows [Ref. 3]:

$$R_H = [(p - \cos\theta)^2 + q^2] / [(p + \cos\theta)^2 + q^2] \quad (18)$$

$$R_V = [(\epsilon' \cos\theta - p)^2 + (\epsilon'' \cos\theta + q)^2] / [(\epsilon' \cos\theta + p)^2 + (\epsilon'' \cos\theta + q)^2] \quad (19)$$

where R_V and R_H , are the vertically and horizontally polarized components of the EM wave, and $\epsilon = \epsilon' - i\epsilon''$; the complex dielectric constant of the surface. The quantities p and q are:

$$p = (1/\sqrt{2})\{[(\epsilon' - \sin^2\theta)^2 + \epsilon''^2]^{1/2} + [\epsilon' - \sin^2\theta]\}^{1/2} \quad (20)$$

$$p = (1/\sqrt{2})\{[(\epsilon' - \sin^2\theta)^2 + \epsilon''^2]^{\frac{1}{2}} + [\epsilon' - \sin^2\theta]\}^{\frac{1}{2}} \quad (20)$$

$$q = (1/\sqrt{2})\{[(\epsilon' - \sin^2\theta)^2 + \epsilon''^2]^{\frac{1}{2}} - [\epsilon' - \sin^2\theta]\}^{\frac{1}{2}} \quad (21)$$

where θ is the incidence angle.

In the case when $\theta = 0$, such as with the viewing angle of the GEOSAT altimeter, R_H and R_V are reduced to the form:

$$\begin{aligned} R_H = R_V &= [(p - 1)^2 + q^2]/[(p + 1)^2 + q^2] \\ &= [(\alpha - 1)^2 + \beta^2]/[(\alpha + 1)^2 + \beta^2] \end{aligned} \quad (22)$$

where the complex index of refraction is given by equation (10). Since $n^2 = \epsilon' - i\epsilon''$, the Fresnel reflection coefficient at normal incidence can take the form:

$$R_V = |(n - 1)/(n + 1)|^2 \quad (23)$$

The spectral emissivity of a surface is related to the spectral reflectivity through Kirchhoff's law (20). We can relate the spectral reflectance R to the emissivity in both horizontally and vertically polarized forms:

$$e_v(\theta) = 1 - R_v(\theta) \quad (24)$$

$$e_h(\theta) = 1 - R_h(\theta) \quad (25)$$

C. BRIGHTNESS TEMPERATURE

The purpose of this section is to develop the relationship between the radiation emitted by the ocean's surface and the upwelling temperature detected by the SSM/I known as the brightness temperature, T_b . All objects, except those existing at absolute zero, emit radiation. An object is classified as a perfect emitter, known as a black body, if it radiates energy at the maximum rate predicted by Planck's radiation law. As the temperature of an object increases, the total amount of energy emitted also

increases. Most objects, however, emit at a rate less than that of a blackbody. The term "grey body", is used to describe an object which emits radiation at a reduced rate. Variations in the temperature of a grey body relative to the assumed blackbody temperature of the earth can be identified and attributed to changes in the environment, such as wind speed, water vapor, and precipitation.

Terms commonly used in discussing brightness temperature, or radiation measurement in general, are radiant energy, radiant flux, irradiance, and emittance. The term radiant energy, Q , refers to the amount of energy carried by the radiation (Joules). The radiant flux, $\Phi = dQ/dt$, is a measure of rate of energy transport (Joules/sec). This flux defines the power available to produce a response in a measuring device. The irradiance, $E = d\Phi/dm^2$, is used in reference to the radiance incident on a surface. The radiance emitted from a surface is known as the emittance, $M = d\Phi/dt$. The character of the material from which radiation is either emitted or reflected is known as its emissivity. Each surface has a particular value, for example, the emissivity of salt water is 0.3, while that of dry soil is 0.92. It is this difference in emissivity that allows the SSM/I to distinguish between land and sea surfaces.

The GEOSAT relies on the degree of reflectivity to detect changes in the ocean's surface. The GEOSAT and SSM/I observations are linked by Kirchoff's law, which relates emissivity and reflectivity in the following manner:

$$e = 1 - r \quad (26)$$

where r is the reflectivity of the surface and e is the emissivity.

The ratio of spectral brightness emitted in a direction (θ, ϕ) by a real body relative to that which is radiated by a blackbody is the spectral directional emissivity

e of that body, where ϵ is a function of wavelength λ and spherical angles ϕ and θ . The microwave emission from the ocean surface is given by ϵB_v , where B_v follows the Rayleigh-Jeans approximation of Planck's Law. Planck's Law states that the spectral brightness per unit of frequency is expressed as:

$$B_v = (2hv^2/c^2) (1/[e^{(hv/kT)} - 1]) \quad (27)$$

where:

$k = 1.38 \times 10^{-23}$ J/K, Boltzman's constant

$h = 6.63 \times 10^{-34}$ J s, Planck's constant

$T \equiv$ temperature in degrees Kelvin

$v \equiv$ frequency of radiation in hertz

$c = 3 \times 10^8$ m/s, speed of light in a vacuum

The Rayleigh-Jeans approximation is made at microwave frequencies, where $hv/(kT) \ll 1$, so that:

$$e^{(hv/kT)} = 1 + hv/(kT)$$

Substituting the above relationship into equation [18] gives

$$B_v = (2v^2k/c^2)T \quad (28)$$

Equation [19] states that the spectral brightness is proportional to the temperature of the body emitting radiation. The radiance received by a microwave sensor is known as the brightness temperature. The brightness temperature T_b , is given by ϵT and will be discussed in a later chapter.

The following section will cover the topics of absorption and the interaction of radiation with surfaces. These factors contribute to the variation in brightness temperatures as measured from satellites.

D. ABSORPTION AND SCATTERING OF RADIATION

Radiation emitted by the ocean surface must pass through the atmosphere once before being detected by the SSM/I, and twice for the GEOSAT altimeter. Consequently, interactions which take place between the atmosphere and the radiation must be understood in order to interpret a retrieved signal. In the atmosphere, energy is both scattered and absorbed. For microwave frequencies, the primary absorber is water vapor, while scattering is predominantly due to rain. Any instrument used to measure wind speed over the ocean must utilize frequencies where the effects of atmospheric absorption and scattering are small. The GEOSAT altimeter frequency was chosen such that atmospheric effects would be small. In addition to observing the ocean surface, the SSM/I measures atmospheric parameters such as water vapor and precipitation. This allows the SSM/I to adjust for atmospheric parameters which would interfere with the measurement of wind speed. Questionable wind speeds, based on the presence of these interfering parameters, are identified at ground stations when the data is analyzed.

E. THE RELATION OF SURFACE ROUGHNESS TO EMITTED RADIATION

The roughness of the ocean causes the reflected and emitted EM waves to be sent out in numerous directions. Remote sensors of microwave radiation must be able to account for this variation in directionality, hence the viewing angle becomes an important factor. The received radiation is also a function of the dielectric constant

of the surface. These properties can be related if we, (1) assume that the surface is made up of many small facets, (2) examine only a single facet, or plane dielectric surface and apply the Fresnel Reflection Coefficients to that surface to obtain the spectral reflectance of that surface. Finally, (3) integrate over all the facets in the area observed by the sensors to obtain the spectral reflectance for that surface.

The solution to the Fresnel equations requires that either the complex dielectric constant, ϵ_r , or the index of refraction of the surface as a function of frequency be known. In the case of the ocean, the dielectric constant is a well known parameter through the work of Lane and Saxon [Ref. 4]. The dielectric constant is represented by the Debye equation:

$$\epsilon_r = \epsilon_\infty + [(\epsilon_s \epsilon_\infty)/(1 + (i\omega\tau)^{1-\alpha} - i\sigma/\omega\epsilon_s)] \quad (29)$$

where:

$\omega = 2\pi f$, radiation frequency

$\epsilon_\infty \equiv$ dielectric constant at infinite frequency

$\epsilon_s \equiv$ the static dielectric constant

$\tau \equiv$ the relaxation time

$\sigma \equiv$ the ionic conductivity

$\alpha \equiv$ an empirical constant

The parameters ϵ_s , τ , and σ are all functions of the material which is reflecting or emitting the radiation to be received by microwave sensors. The conductivity σ of the sea water increases the complex portion of the dielectric constant, however, it is important to note that the influence of sea salts on the emissivity of the ocean is small

for frequencies greater than 5 GHZ. Since both the SSM/I and GEOSAT sensors operate above 5 GHZ, the salinity of the sea water has no effect.

The above description for spectral reflectance and emittance from a single facet can now be applied to the entire rough surface. This is accomplished by integrating over all the facets and taking a statistical average.

F. THE RADIATIVE TRANSFER EQUATION

The radiative transfer equation contains terms which relate radiant energy from the surface and atmosphere to the radiant energy observed by a satellite. Before energy can reach a satellite sensor from the ocean surface, the upwelling radiation is attenuated and joined by additional emission from the atmosphere, so that the observed temperature detected by the SSM/I is given by:

$$T = T_A(1 - t) + t[eT_s + (1 - e)(1 - t)T_A] \quad (30a)$$

or

$$T = et[T_s - T_A(1-t)] + T_A(1 - t^2) \quad (30b)$$

where, T_A is the effective temperature of the atmosphere, $t = e^{-\tau}$, τ is the optical depth, T_s is the sea surface temperature, and e is the emissivity. The brightness temperature of the radiation incident on the ocean surface by the atmosphere is $T_A(1-t)$. The amount that is reflected by the sea surface is written as $(1 - e)T_A(1 - t)$, while the amount emitted is eT_s . It follows that the total upwelling brightness temperature from the sea surface is $eT_s + (1 - e)(1 - t)T_A$. The signal from the surface is eT_s . The other terms are considered noise with regard to surface wind

speed analysis, but are useful when detecting water vapor, liquid water, and precipitation. If the optical depth $\tau = 0$, then the atmosphere is transparent and allows just the brightness temperature of the ocean surface to be seen by the sensor. Equation (30b) would then be reduced to simply $T = eT_s$. This is the ideal case for measuring wind speed over the ocean. If, on the other hand, $\tau \gg 0$, then $T = T_a$, i.e., the SSM/I would be looking at the environmental changes in the atmosphere only. The frequencies and the method used by the SSM/I and GEOSAT to minimize atmospheric interference will be discussed in sections devoted to instrument operation.

G. THE TRANSFER OF MOMENTUM FROM THE ATMOSPHERIC SURFACE LAYER TO THE SEA SURFACE

Waves and foam generated by the wind contribute to the roughness of the sea surface and effect both microwave emission as measured by the SSM/I and microwave scattering as measured by the GEOSAT altimeter. The roughness has the effect of altering the incidence angle of radiation being emitted or reflected and changing the emissivity of the sea surface itself. The roughness of the sea surface is an indication of the transfer of momentum into the sea from the turbulent atmospheric surface layer. An extrapolation process is performed to relate the wind speed in the atmospheric surface layer to the sea surface roughness. This section will briefly describe the transfer of momentum from the atmospheric surface layer to the sea surface.

Businger [Ref. 5] describes the formulation of the turbulent transfer of momentum from the atmospheric surface layer to the sea surface as a semi-empirical relationship.

The appropriate equation can be developed by utilizing the turbulent transfer coefficient K in the equation for momentum transfer, where:

$$F_m = -\rho K \partial \bar{U} / \partial z \quad (31)$$

Here, ρ is the density and \bar{U} is the mean horizontal wind speed. Businger defines the atmospheric surface layer as the lower 20 meters of the atmosphere. Here the interaction with the surface is strong and the layer adjusts to the surface conditions rapidly. We can therefore assume a quasi-steady-state. The momentum transferred through to the ocean surface exerts a drag force per unit area on that surface known as the surface stress τ . By Newton's third law, the momentum equation is given as:

$$F_m = \overline{\rho u'w'} = -\tau \quad (32)$$

The friction velocity u_* is commonly used as a scaling velocity, where:

$$u_* = (\tau/\rho)^{1/2} \quad (33)$$

Equation (31) can now be written as:

$$K_m \partial \bar{U} / \partial z = u_*^2 \quad (34)$$

where u_* is independent of height. To generate a wind profile from the surface to a height of 20 meters, an assumption must be made about K_m . By dimensional analysis, K_m has the dimensions of velocity times length. We use u_* to scale the velocity and z to scale the length. Therefore, we assume that:

$$K_m = k u_* z \quad (35)$$

where, k is a constant of proportionality, the von Karman constant. Combining equations (34) and (35), we have:

$$\partial \bar{U} / \partial z = u_* / (kz) \quad (36)$$

To avoid an infinite shear at the surface, when $z = 0$, a finite surface roughness z_o is introduced into the equation. This now becomes:

$$\overline{\partial U / \partial z} = u_* / (k[z + z_o]) \quad (37)$$

Upon integration we have the form:

$$\overline{U} / u_* = 1/k \ln[(z + z_o)/z_o] \quad (38)$$

which is the logarithmic profile for the wind from the sea surface through the atmospheric surface in a neutrally stable atmosphere. This is the common profile used to extrapolate surface wind speed to a height of 10 or 20 meters, which are the typical heights at which sea buoys and ships measure wind speed at sea. The neutral case is used primarily for its simplicity and also for its adequate approximation of the surface layer wind field. Figure (3) [Ref. 6] represents a semi-log plot of wind speed from the surface through the atmospheric boundary layer for neutral, stable and unstable conditions. It would be impractical to measure the stability of the atmosphere for all wind speed measurements. Fortunately, the neutral profile of wind speed approximates the atmosphere in most situations.

Fig. 3 is derived from setting equation (37) equal to a wind shear function, Φ_M , such that:

$$\Phi_M = (k[z + z_o]/u_*) \overline{\partial U / \partial z}$$

where:

$$\Phi_M = 1 + [4.7 z/L], \quad \text{for } z/L > 0 \text{ (stable)} \quad (39a)$$

$$\Phi_M = 1 , \quad \text{for } z/L = 0 \text{ (neutral)} \quad (39b)$$

$$\Phi_M = [1 + [15 z/L]]^{-1/4}, \quad \text{for } z/L < 0 \text{ (unstable)} \quad (39c)$$

and L is the Obukhov length.

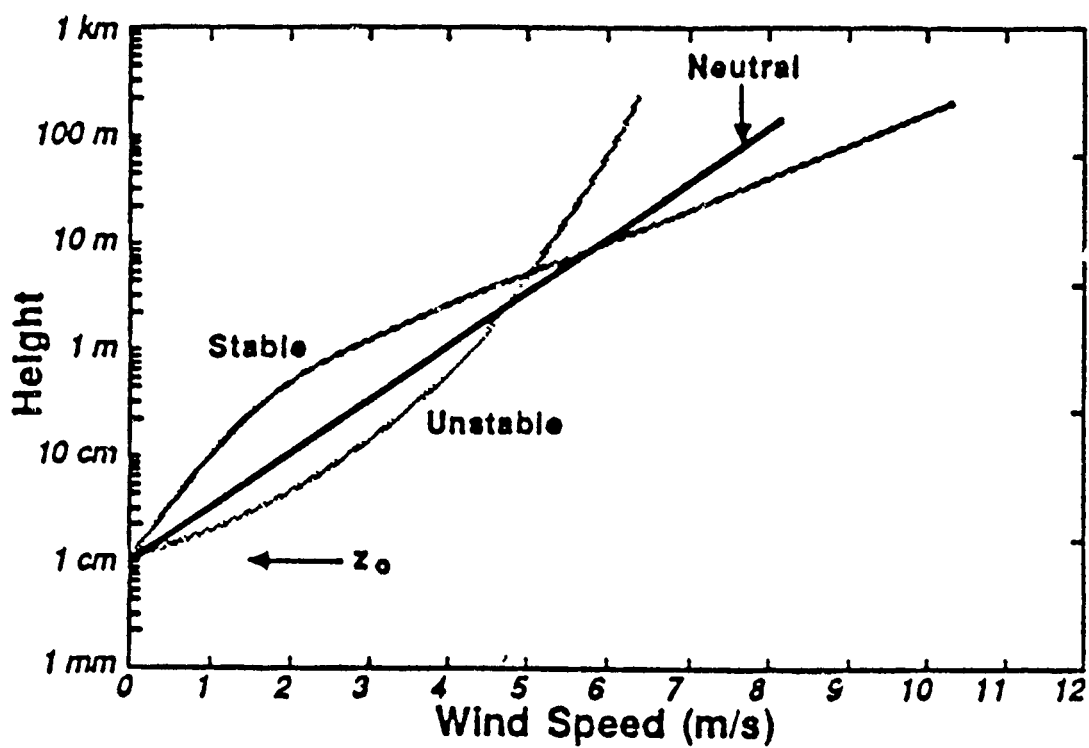


Figure 3 Typical wind speed profiles versus static stability in the surface layer.

III. MEASURING WIND SPEED OVER THE OCEAN WITH THE SSM/I

The SSM/I is a microwave radiometer which measures upwelling radiation from the earth's surface at five frequencies and two polarizations. Using frequencies associated with atmospheric windows, the SSM/I measures upwelling thermal microwave radiation from the ocean surface. This radiation is called the brightness temperature. From equation (30b), where $T_b = eT_s$ for an atmosphere with 100% transmittance, the brightness temperature is a function of the emissivity, e , and temperature of the sea surface, T_s . The sea surface temperature is relatively constant compared to the change in emissivity. An increase in T_b is thus caused by an increase in the sea surface emissivity. A change in surface roughness and thus wind speed, will change the emissivity of the surface. Thus, a particular wind speed at the sea surface can be related to a certain brightness temperature.

The SSM/I utilizes the 19.35H, 22.235V, 37H, and 37V GHz channels for measuring wind speed, where H and V represent horizontal and vertical polarizations respectively. The 19.35H, 37H, and 37V GHz channels are "windows" in which there is nearly 100 % transmission of upwelling radiation through the atmosphere. The 22.235 GHz channel is in the center of a water vapor absorption line and is used to measure water vapor concentration. Detection of water vapor is vital to the determination of the validity of the wind speed detected, since the 19.35H, 37V, and 37H channels are subject to some small amount of atmospheric interference which require that an atmospheric correction be applied.

The algorithm used by the SSM/I for measuring wind speed assumes the roughness of the ocean surface can be treated as a conglomeration of many tiny emitting planes whose angle of inclination is altered by the force of the wind. The variation in the sea surface slope is used in calculating the emissivity of the surface by assuming a Gaussian slope distribution of the angles of the slope. A change in the distribution of these angles corresponds to a change in the root mean square slope of the sea surface and distribution of the emissivities associated with the variance of sea surface slopes. The resulting change in emissivity causes a change in brightness temperature through the Fresnel equations (Eqns.22 and 23). The equation used to describe the dependence of derived wind speed on the surface slope variance, σ^2 [Ref. 7] , is as follows:

$$\sigma^2(f) = (0.3 - 0.02f) (0.003 + 0.48U_{20}) \text{ for } f < 35 \text{ GHz} \quad (40a)$$

$$\sigma^2(f) = 0.003 + 0.48U_{20} \text{ for } f \geq 35 \text{ GHz} \quad (40b)$$

Here, f is defined as the frequency in GHz and U_{20} as the wind speed measured in meters/second at a 20 meter height.

Foam generated by breaking waves occurs at wind speeds greater than 7 m/s. The affect of foam on the microwave emission from the sea surface is not well understood and there are varying theories in literature. Swift [Ref. 8] cites an experiment over the Salton sea using a 19 GHz radiometer to measure wind speed over a foam covered sea. Swift states that the results were tens of degrees higher than theory and could be attributed to the presence of foam. Wilheit [Ref. 9] treated foam

as a relatively non-reflective surface and eliminated it from the radiative transfer equation. The reflectivity that does occur comes from the dielectric interface around the foam bubbles. Hollinger et al [Ref. 10] treat foam as "a substance which partially obscures the ocean surface in a manner independent of polarization but dependent upon frequency". He defines the foam fraction, F_f , as

$$F_f = 0.006 (U_{20} - 7) (1 - e^{-0.75}) \quad \text{for } U_{20} > 7 \text{ m/sec} \quad (41a)$$

$$F_f = 0 \quad \text{for } U_{20} \leq 7 \text{ m/sec} \quad (41b)$$

This equation is developed from the observation that the sea surface brightness temperature increases linearly for wind speeds in excess of 7 m/sec, and that there is an absence of foam development for speeds less than or equal to 7 m/s. The foam fraction is also used in the empirically derived SSM/I wind speed algorithm to account for the change in emissivity that occurs with the presence of foam.

IV. MEASURING WIND SPEED OVER THE OCEAN WITH THE GEOSAT ALTIMETER

The primary mission of the GEOSAT satellite was not wind measurement, but measurement of the geoid and sea surface height. However, wind is computed as a by-product and with an accuracy of ± 2 m/s [Ref. 10]. To measure wind speed, the GEOSAT satellite utilizes an active radar operating at a frequency of 13.9 GHz called an altimeter. This instrument transmits a pulse of microwave energy to the ocean surface and measures the return signal. The altimeter [Ref. 11] uses an automatic gain control (AGC) loop to normalize the amplitude of the return signal from the sea surface. The AGC is a measure of the backscatter cross section of the sea surface, σ , and is related to the wind speed. The greater the wind speed, the lower the cross section, thus the weaker the return signal from the ocean surface. The backscatter cross section is obtained from the following equations [Ref. 12]:

$$\text{AGC [dBm]} = 10 \ln (P_r/P_o) \quad (43)$$

where:

P_r \equiv the received power

P_o \equiv the reference power (1 mW)

The received power P_r , is defined in terms of antenna gain G , transmitted power P_t , the operating wavelength λ , the distance to the sea surface R , and the scattering cross section σ . The relation appears as follows:

$$P_r = [\lambda^2/(4\pi)] P_t G \sigma / R^4 dA \quad (44)$$

Assuming that the sea surface slope is both gaussian and isotropic in its probability distribution, we can define σ as follows:

$$\sigma = [|R(0)|^2 / S^2] \sec^4 \Theta \exp [-\tan^2 \Theta / S^2] \quad (45)$$

where:

$\Theta \equiv$ angle of incidence

$R(0) \equiv$ Fresnel reflection coefficient for the air-sea interface at normal incidence

The Cox and Munk [Ref. 13] relationship for average upwind/crosswind mean square sea surface slope σ^2 and wind speed is given as:

$$\sigma^2 = \alpha + \beta U \quad (46)$$

where, U is the wind speed in m/s and α , β are empirical constants of proportionality which depend on the probability density of the sea surface slope. By making the assumption of an isotropic Gaussian surface, the separate effects of the upwind component and the crosswind component are ignored [Ref. 14]. By ignoring wind direction when deriving a relationship between wind speed and surface slope, error in the surface wind speed will be introduced.

If we let $\Theta = 0$, since we are observing at the nadir angle, the equation for σ becomes:

$$\sigma = |R(0)|^2 / (\alpha + \beta U) \quad (47)$$

The equation for the received power is

$$P_r = (\lambda^2 / (4\pi)^3) P_t (G^2 / h^4) \sigma A \quad (48)$$

where:

$h \equiv$ satellite altitude

$A \equiv$ area illuminated by the altimeter

This relationship is used in the Brown algorithm for the actual calculation of wind speed [Ref. 15] at the Fleet Numerical Oceanographic Center. Brown's algorithm is a result of a comparison of wind speed data received from sea buoys to normalized backscattered cross sections derived from altimeter power measured on board the

GEOS-3 satellite and applied to GEOSAT. The algorithm is presented in two stages. The first section is as follows:

$$W_1 = \exp [(10^{(0.21 \times \sigma'/10)} - B)/A] \quad (49)$$

where:

$$A = 0.080074 \quad B = -0.124651 \quad \text{for } \sigma' < 10.12 \text{ dB}$$

$$A = 0.039893 \quad B = -0.031996 \quad \text{for } 10.12 \leq \sigma' \leq 10.90 \text{ dB}$$

$$A = 0.015950 \quad B = 0.017215 \quad \text{for } \sigma' \geq 10.9 \text{ dB}$$

In the above equation, the backscattered cross section is given as decibels relative to 1 m².

A second equation is used to complete the derivation of surface wind speed. This was necessary to adjust for the skewness in the distribution of the differences between the buoy and altimeter wind speed measurements. The second part of the algorithm is as follows:

$$U_{10} = \sum_{n=1}^5 a_n W_1^n, \quad \text{for } W_1 \leq 16 \text{ meters per second} \quad (50a)$$

$$U_{10} = W_1, \quad \text{for } W_1 > 16 \text{ meters per second} \quad (50b)$$

where:

$$a_1 = 2.08779900000$$

$$a_2 = -0.36499280000$$

$$a_3 = 0.04062421000$$

$$a_4 = -0.00190495200$$

$$a_5 = 0.00003288189$$

U_{10} is the wind speed at a height of 10 meters. This algorithm appears to measure the wind to within +/- 2 m/s.

V. GROUND TRUTH STUDIES

A. GEOSAT Wind Speed Ground Truth Study

Shuhy [Ref. 16] made a ground truth study for the wind speeds obtained by GEOSAT using National Data Buoy Center buoy data. To avoid possible interference from land, most of the buoys used were located in deep water away from any coastlines. Shuhy chose to restrict the comparison to satellite passes within 80 kilometers and 90 minutes of a ground truth point. The data was classified as either excellent, good, or fair based on the following criteria:

<u>CLASSIFICATION</u>	<u>DISTANCE FROM GROUND TRUTH</u>	<u>TIME DIFFERENCE IN OBSERVATIONS</u>
excellent	25 KM	30 min
good	25 - 60 KM	60 min
fair	60 - 80 KM	90 min

No data outside 80 kilometers or 90 minutes from crossing were used. The results of the comparison are seen in Fig. 4. Shuhy concluded from regression analysis that the sub-categorization described above yielded no significant differences. A total of 256 data points were used with an rms error of 1.54 m/s. The comparison demonstrated that GEOSAT wind speeds are higher than the ground truth for speeds less than 6 m/s and for speeds greater than 6 m/s, GEOSAT winds are lower than those obtained on the surface. Shuhy notes, however, that there is significant scatter in the data and that

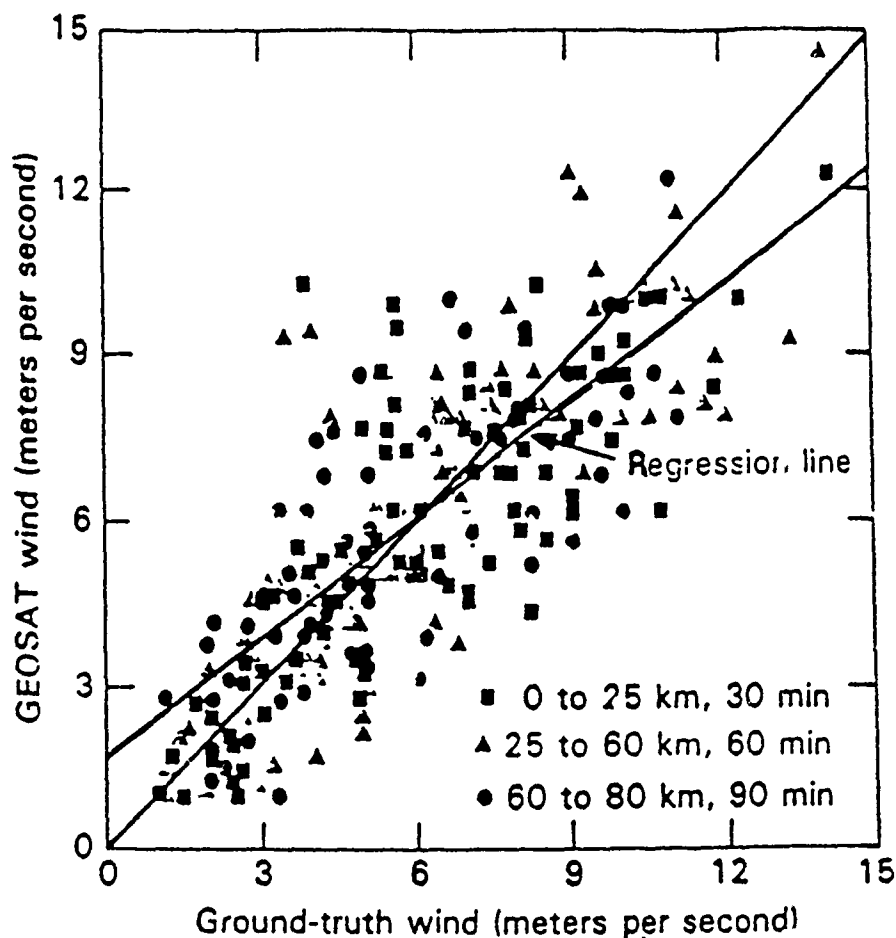


Figure 4 Geosat vs ground truth winds at a height of 10 meters.

spatial variability must be examined to determine which comparisons might be invalid due to high variability between buoy and satellite wind speeds along the satellite track.

When ground truth data is compared to off-nadir GEOSAT data, there appears to be a correlation between the magnitude of the angle and how well the GEOSAT and buoy wind speed compared. For angles greater than 1.1 degrees, the correlation was poor. Angles less than 0.4 degrees off nadir exhibited good correlation in the GEOSAT/buoy wind speed comparisons. In this study, the nadir angle was not

available as the GEOSAT data used was preprocessed by Naval Ocean Research and Development Activity (NORDA), however all data with off nadir angles greater than 1° is not transmitted to FNOC.

B. SSM/I WIND SPEED GROUND TRUTH STUDY

The SSM/I algorithms have undergone four revisions since the system was put into space in late 1987. The study completed by Hollinger and Poe [Ref. 18] includes 600 SSM/I and buoy data sets. Comparisons of wind speed measurements were made within 30 minutes and 25 kilometers of each other (Fig. 5).

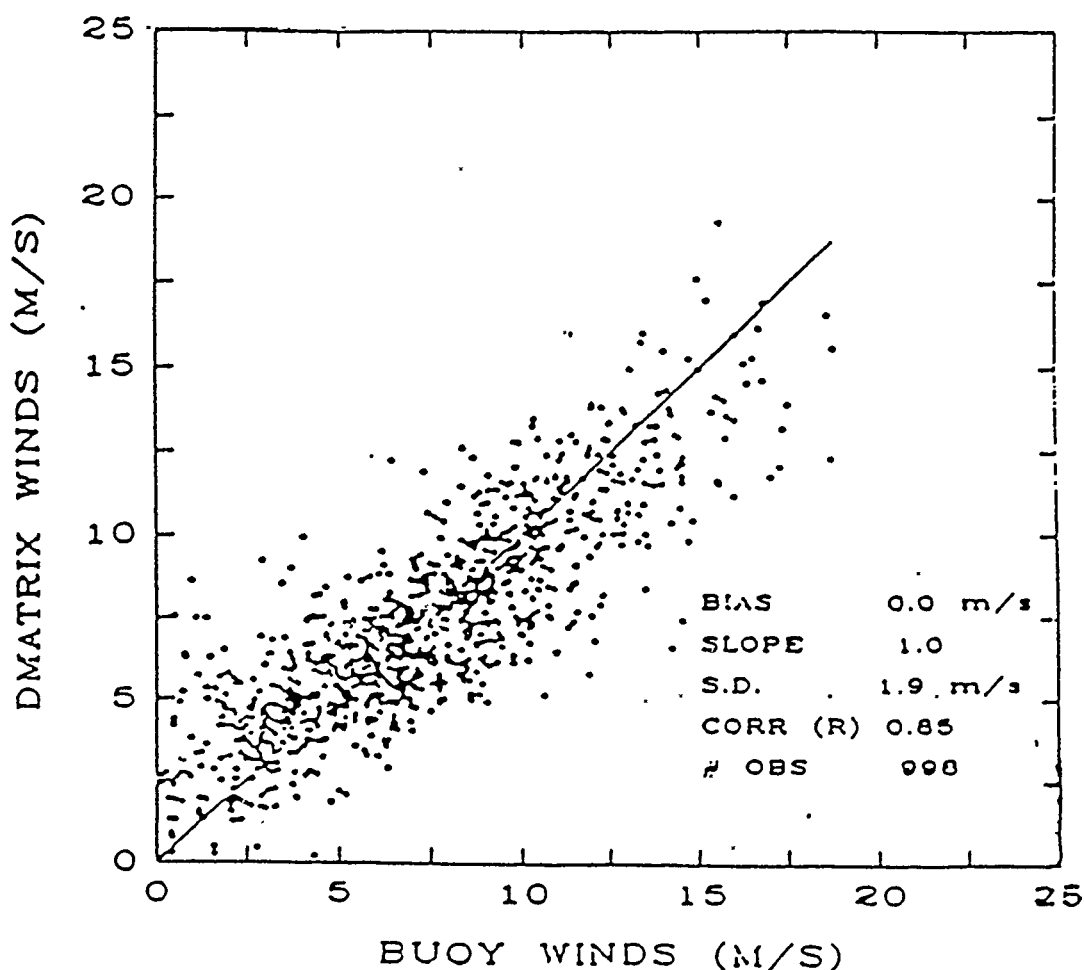


Figure 5 SSM/I wind speed comparison with ground truth from moored buoys (Hollinger and Poe).

The SSM/I winds are extracted from a data set by the "D-matrix" method. This is an empirical/statistical approach that chooses the most probable atmospheric and surface conditions that would produce a characteristic set of measured brightness temperatures. The "D-matrix" contains the reference brightness temperatures for the SSM/I. The SSM/I retrieved brightness temperatures are compared to the "D-matrix" and from this comparison the ocean and atmospheric conditions that were observed by the SSM/I are determined. The overall scatter of data points represents a ± 2 m/s standard deviation between 3 and 15 m/s. At this time, there is insufficient data for wind speeds greater than 15 m/s to make an accurate comparison of SSM/I and buoy wind speeds.

Interfering factors that could reduce the accuracy of the analysis are heavy concentrations of water vapor and the presence of cloud water and rain. In this study, areas exhibiting these conditions were included in the data to observe their influence on retrieved wind speeds.

Positioning error was discovered by as much as 20 to 30 km for shift in pixel latitude and longitude coordinates. However, Hollinger and Poe state that this did not interfere with the overall validation of the wind speed algorithm.

VI. SSM/I AND GEOSAT ALTIMETER WIND SPEED COMPARISON

A. DATA ACQUISITION

The data base used was acquired from Fleet Numerical Oceanography Center (FNOC) in Monterey, California. All data obtained for this study was gathered in near-real time using a personal computer (PC) with a 1200 baud modem. Co-located passes of the DSMP and GEOSAT satellites within one hour of each other were required. The position and time of ascending node for the orbits of each satellite were calculated well in advance. These orbit tables were updated every two weeks to account for errors in calculating the exact times of ascending node crossings. Adjustments had to be made to the GEOSAT orbit table to account for the periodic maneuvering of the satellite that would keep it in a 17 day repeat orbit pattern. To avoid any microwave interference from land stations, areas over the open sea were chosen.

Several problems were encountered in obtaining data in this manner. The average length of time to download a single SSM/I data set was at 1200 baud was approximately 0.5 to 1 hour, depending on its size. Near real time SSM/I and GEOSAT data at FNOC is accessible for 6 hours or less before it is removed from memory. As a result, many data sets obtained were incomplete as the data had been removed during the downloading process. I was unable to determine at what times a particular orbit would be resident at FNOC and for what length of time it would be resident. I consequently worked with the data available at the time. Another difficulty

arose in the form of the GEOSAT data format. The GEOSAT data obtained from FNOC was pre-processed by NORDA in Bay St. Louis, Mississippi. The format of the GEOSAT data base included only the latitude, longitude, wind speed, and significant wave height. Raw data would have been ideal, so that various wind speed algorithms could have been tested. Occasionally incomplete data sets were obtained where wind speeds were missing for large areas of an orbit. This was due to data transmission problems occurring between NORDA and FNOC. Despite these difficulties, five data sets were obtained from three different regions of the globe: the North Atlantic, the Gulf of Alaska, and a region in the North Central Pacific.

B. DATA FORMATS AND PROCESSING

This section describes the various formats in which the SSM/I and GEOSAT data are found. In addition, the process in which raw SSM/I information is decoded and then combined with the preprocessed GEOSAT wind speeds to form the final data base will be discussed.

1. SSM/I Data Base

There are four forms of data which are on file for each orbit made by the DSMP satellite. All are encoded in hexadecimal format and must be decoded to decimal before processing.

The Orbit Summary File (SUM) contains information on the latitude and longitude of each end of the sensor swath for entire satellite orbit. Included with this is a history of sensor health, i.e., whether or not any of the sensors on board experienced any unusual fluxes in radiation, including the hot calibration standard,

reference voltages, and the automatic gain control. From this file, the exact time during which the DMSP orbit would coincide with a GEOSAT crossing could be determined. This fixed the amount of data needed to be downloaded to cover as much of the GEOSAT track as possible.

Raw brightness temperatures for each sensor, are initially stored in a file known as the Sensor Data Record (SDR). An Antenna Pattern Correction (APC) is applied to the brightness temperatures to correct for spurious energy received in the side lobes. Corrected brightness temperatures are then stored in the Temperature Data Record (TDR). It is in this format that brightness temperatures can be used to derive geophysical data such as precipitation rates, ice edge, ice age, water vapor, and wind speed. The geophysical data are then stored in the Environmental Data Record (EDR). This is the level of data used in this study.

2. GEOSAT Data Base

GEOSAT altimeter data is stored on board the satellite for approximately 12 hours and then transmitted to a receiving station at the Johns Hopkins Applied Physics Laboratory (APL) where it is archived on tape. Three data products are produced from the raw data; The Sensor Data Record, the Naval Ocean Research and Development Activity (NORDA) Data Record, and the Waveform Data Record. The first two contain information about the measured altitude, significant wave height, wind speed, automatic gain control, and corrections for satellite and instrument errors. The last record contains waveform data used primarily for ice studies.

FNOC stores GEOSAT data received from NORDA in half hour blocks which contain latitude, longitude, wind speed, and sea surface height information.

The data is pre-processed and does not contain the raw data necessary to verify the algorithms used to produce the wind speeds and corrections made to the data set. Reliance was placed on the ground truth comparison made with the GEOSAT wind speed calculations to establish the validity of the wind speed data.

3. Processing GEOSAT Altimeter and SSM/I data sets

Several Fortran programs were used to convert the hexadecimal format of the SSM/I data records to decimal. A program called COMPARE was written to combine the measurements from both the GEOSAT and SSM/I EDR data bases for each co-located satellite pass. SSM/I wind speeds measured within a 0.25 degree radius of a GEOSAT data point were averaged together and a mean value and standard deviation were obtained. A new data set was then produced which contained the GEOSAT wind speeds and the mean values of the SSM/I wind analysis from which correlation studies were made. A graphical representation of the two data sets were produced. The SSM/I EDR also supplied the rain, cloud water, and water vapor analysis necessary to determine the environmental conditions that existed during the wind speed measurements.

C. DATA ANALYSIS AND RESULTS

A comparison of all the compiled data sets for the SSM/I and GEOSAT altimeter wind speed analysis is seen in Fig. 6. The correlation for the compiled data sets is 0.703. From this graph, four distinct regions are seen. The region "A" extends from 2.5 to 9 m/s. Here, the SSM/I demonstrated good correlation with the GEOSAT altimeter. Wind speeds between 5 and 8 m/s represent compiled data from four

different orbits, however, wind speed from 2.5 to 5 m/s was derived from a single data set, which resulted in a region of sparse data. The SSM/I is limited to a minimum detectable wind speed of 3 m/s. This limitation is due to the lack of sensitivity to changes in emissivity for wind speeds between 0 and 3 m/s. The region greater than 8 m/s demonstrated very poor correlation between the SSM/I and the GEOSAT altimeter. This area is divided into three separate regimes. The region "B" corresponds to the bulk of data which is greater than 9 m/s. Here, the correlation appears to be good, but the SSM/I data are notably biased to the higher wind speeds. On either side of region "B", there are outlying points. Region "C" is identified by the extremely high values of wind speed of the SSM/I for GEOSAT winds from 8 to 12 m/s. Region "D" is represented by the high values of the GEOSAT wind speeds relative to the SSM/I values from 11 to 14 m/s.

As both systems have successfully verified wind speeds in the regime between 8 to 15 m/s, the regions where the two measurements differed were examined in detail. The water vapor, cloud water content, and rain measured by SSM/I were used to determine if any interference due to these substances may have caused the bad correlation in the high wind speed areas. This was done for each individual data set to determine if regional differences may have made a contribution. Data sets are identified by the corresponding SSM/I orbit number, latitude and longitude of the region, as well as the date and time difference between the SSM/I and GEOSAT co-located orbits.

SSM/I VS ALTIMETER WIND SPEED

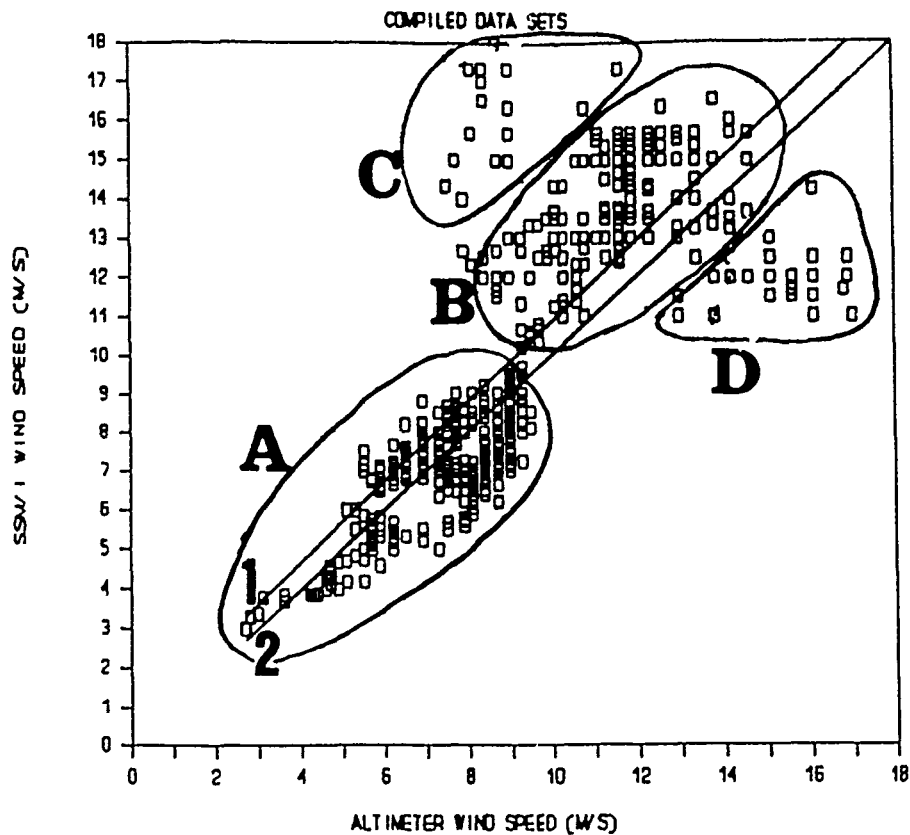


Figure 6 SSMI versus GEOSAT wind speeds in meters per second. Line number 1 represents the actual correlation of 0.703 and line 2 represents a reference correlation of 1.0.

1. Orbit 9138, 27 March, 1989

The scan area of the SSM/I encompassed a region bounded by the following coordinates:

<u>Latitude</u>	<u>Longitude</u>
32.50°N	226.00°E
32.50°N	242.20°E
17.00°N	226.00°E
17.00°N	242.20°E

The time difference between the GEOSAT and SSM/I passes is no greater than 0.61 hours. The track of the GEOSAT through the SSM/I swath begins at 20°N,231.8°E and ends at 29.5°N,227.4°E. The wind speeds recorded in this region ranged from 2.8 to 7.9 m/s. The correlation for this pass is 0.925 (Fig. 7). The difference in wind speed for the individual satellites demonstrates a maximum of 1.9 m/s (Fig. 8). The wind field, as observed by the SSM/I, is depicted in Fig. 9. The entire area of co-located orbits reveals a region of high water vapor content of approximately 60 kg/m² (Fig. 10). No cloud water or precipitation is present in this region. Since the correlation of the wind speed for orbit 9138 is so high, one could safely deduce that a water vapor content as high as 60 kg/m² does not adversely affect the remote sensing of wind speeds by microwave instruments.

2. Orbit 8934, 13 March, 1989

The scan area of the SSM/I encompassed a region bounded by the following coordinates:

<u>Latitude</u>	<u>Longitude</u>
57.94°N	214.33°E
54.44°N	192.55°E
47.39°N	216.97°E
44.57°N	199.38°E

The time difference between the GEOSAT and SSM/I passes is within 1.01 hours. The track of co-located orbits begins at 39.5°N,217.8°E and ends at 27.8°N,211.5°E.

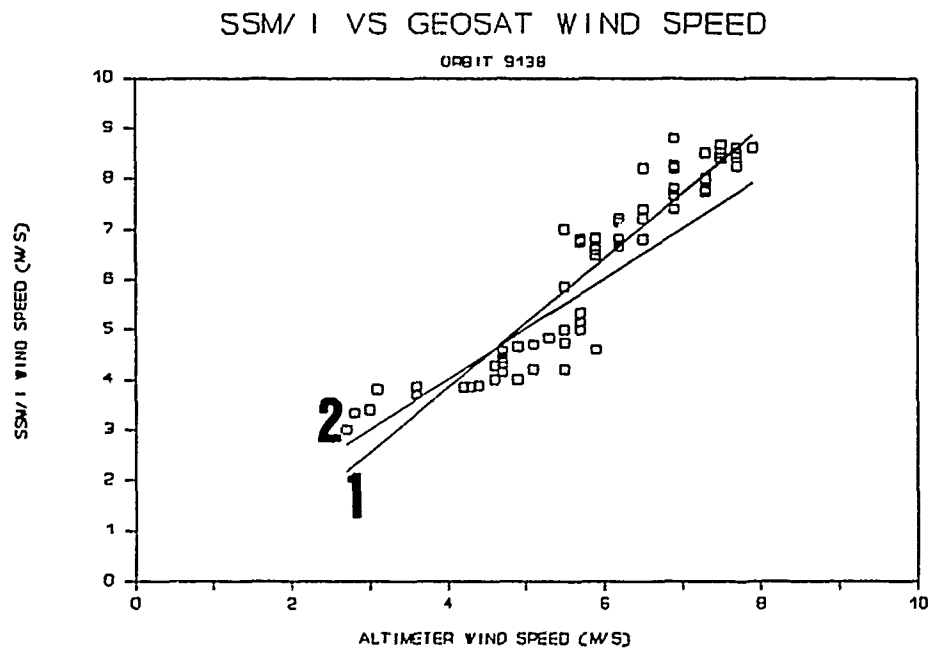


Figure 7 SSM/I vs altimeter wind speed. Line number 1 represents the actual correlation of 0.925 and line 2 represents a reference correlation of 1.0.

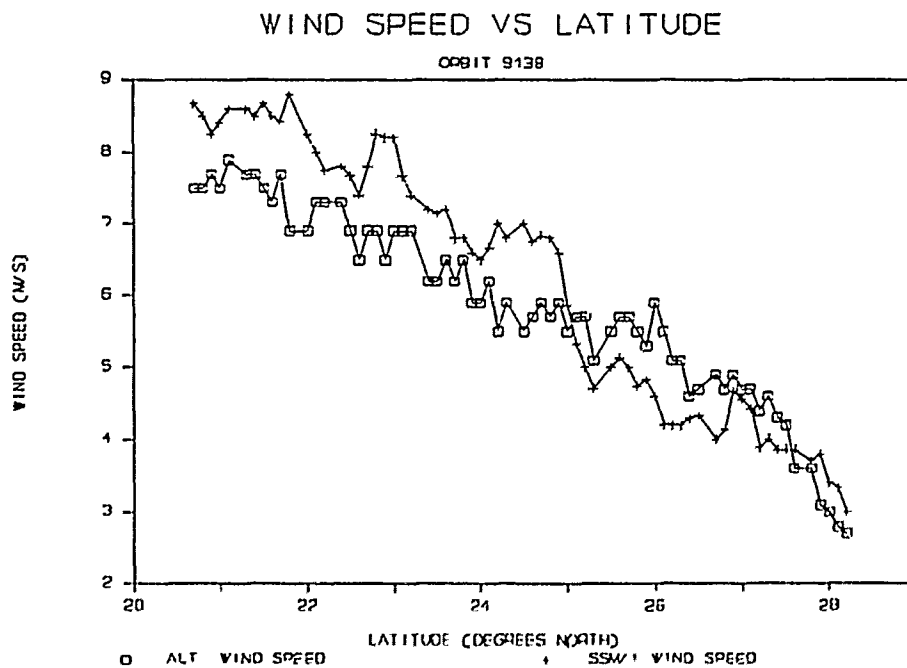


Figure 8 SSM/I and GEOSAT wind speed vs. latitude: orbit 9138.

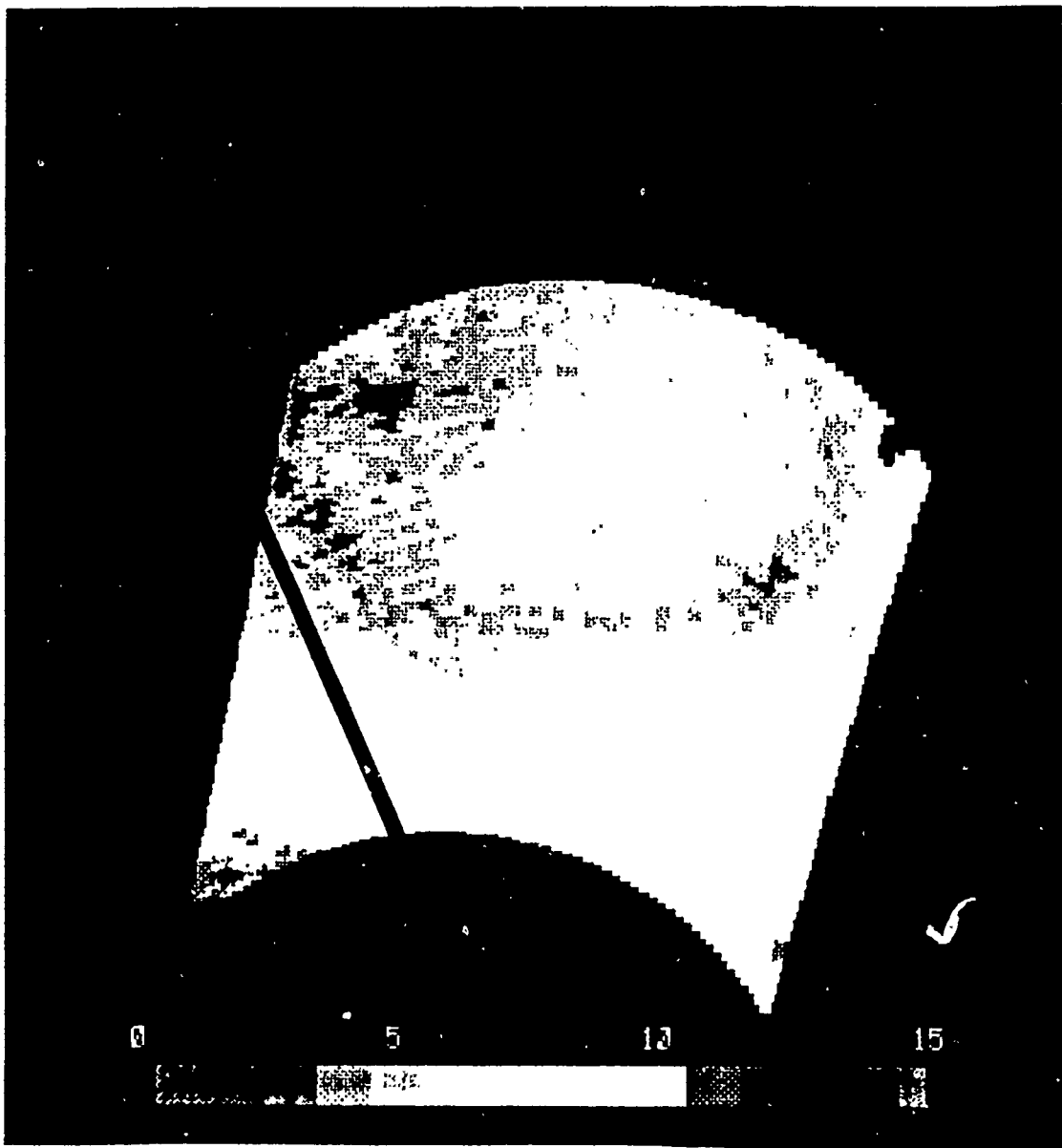


Figure 9 SSM/I wind speed field (m/s); orbit 9138. Line through field represents GEOSAT flight path.

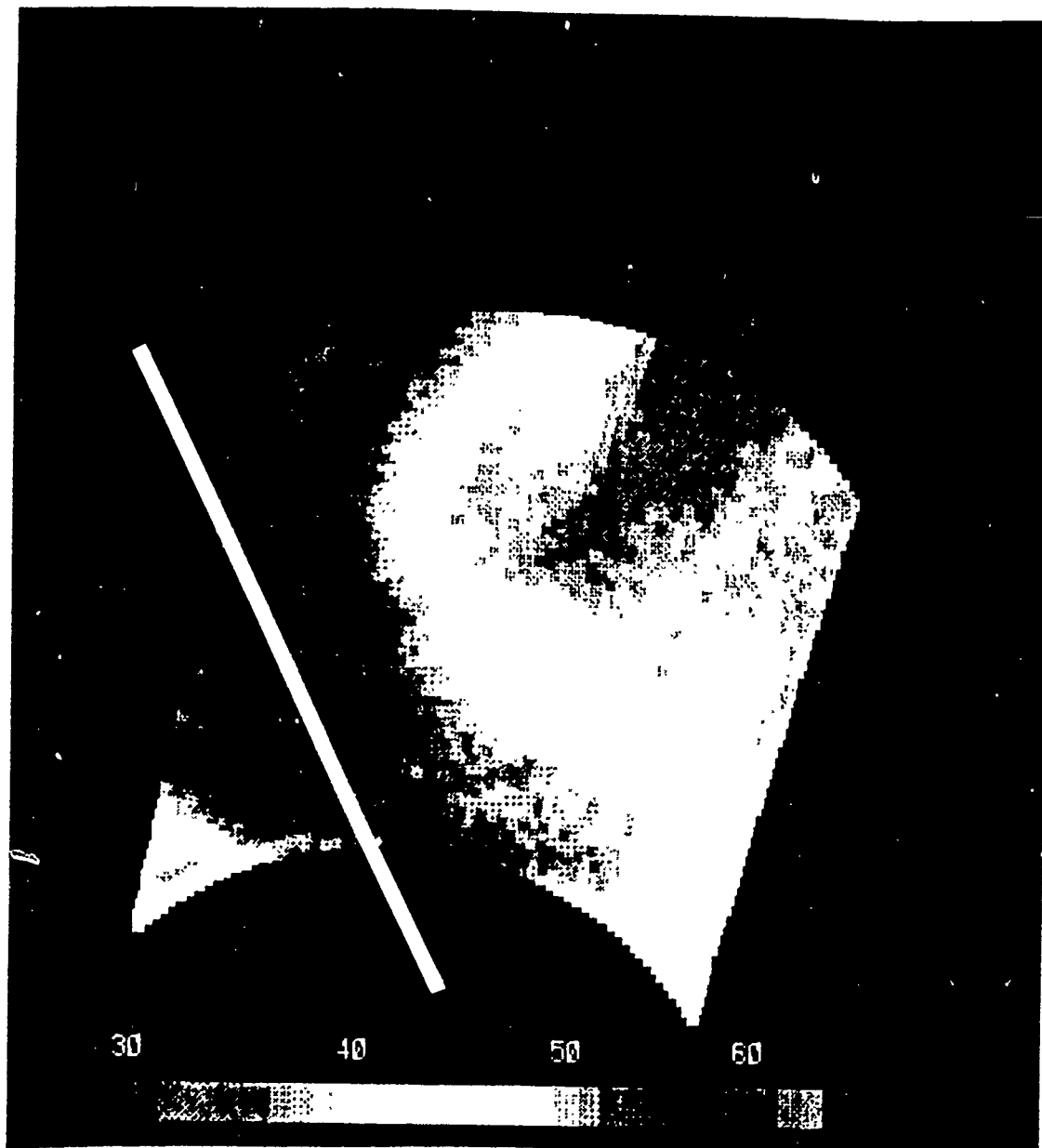


Figure 10 SSM/I water vapor field (kg/m^2); orbit 9138. The line through the field represents the GEOSAT flight path. A high correlation of wind speeds exist between the GEOSAT altimeter and SSM/I despite high water vapor concentration.

A break in the track was due to an interruption in communications during the transfer of data over a modem. Data were consequently lost between 31°N and 32.5°N latitudes. The statistics for this orbit revealed a correlation between the GEOSAT altimeter and SSM/I wind speeds of 0.616. This data set spans a range of wind speeds from 5 to 9.5 m/s (Fig. 11). The data points appear to be slightly biased toward the higher wind speeds for the GEOSAT altimeter. The plot of wind speed versus latitude (Fig. 12) reveals that both satellites follow the trend of increasing and decreasing wind speeds. The largest difference in wind speeds (approximately 2.5 m/s) appears at 29.2°N, 32.5°N, 35.5°N, and 38°N latitudes. The images of wind speed (Fig. 13), water vapor (Fig. 14), and precipitation (Fig. 15) show that the track of the co-located orbit does not pass through any interfering atmospheric substances and that there were no unusual gradients in the vicinity. Overall, orbit 8934 demonstrated good correlation between the GEOSAT altimeter and the SSM/I.

3. Orbit 8058(7), 10 January, 1989

The scan area of the SSM/I encompassed a region bounded by the following coordinates:

<u>Latitude</u>	<u>Longitude</u>
59.73°N	217.54°E
57.84°N	197.63°E
51.88°N	223.64°E
48.89°N	205.01°E

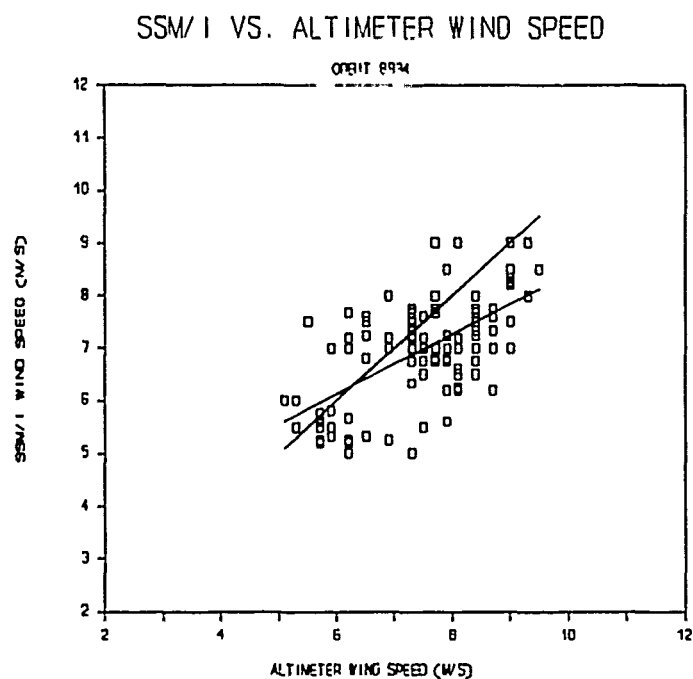


Figure 11 SSM/I vs. GEOSAT WIND SPEED: ORBIT 8934. Line 1 represents the linear regression line. Line 2 is a reference slope of 1.0.

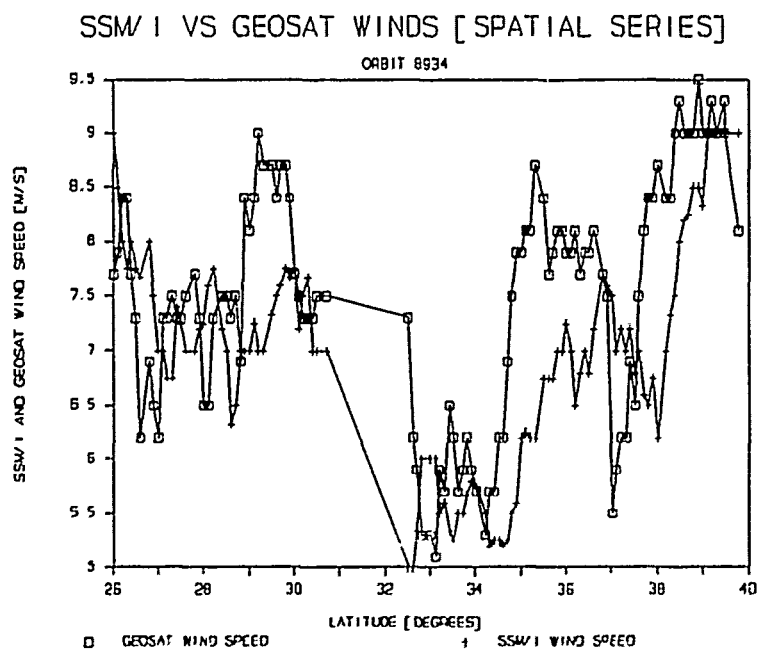


Figure 12 SSM/I and GEOSAT winds vs latitude: orbit 8934.



Figure 13 SSM/I wind speed field (m/s); orbit 8934. Line through the wind field represents the GEOSAT flight path.

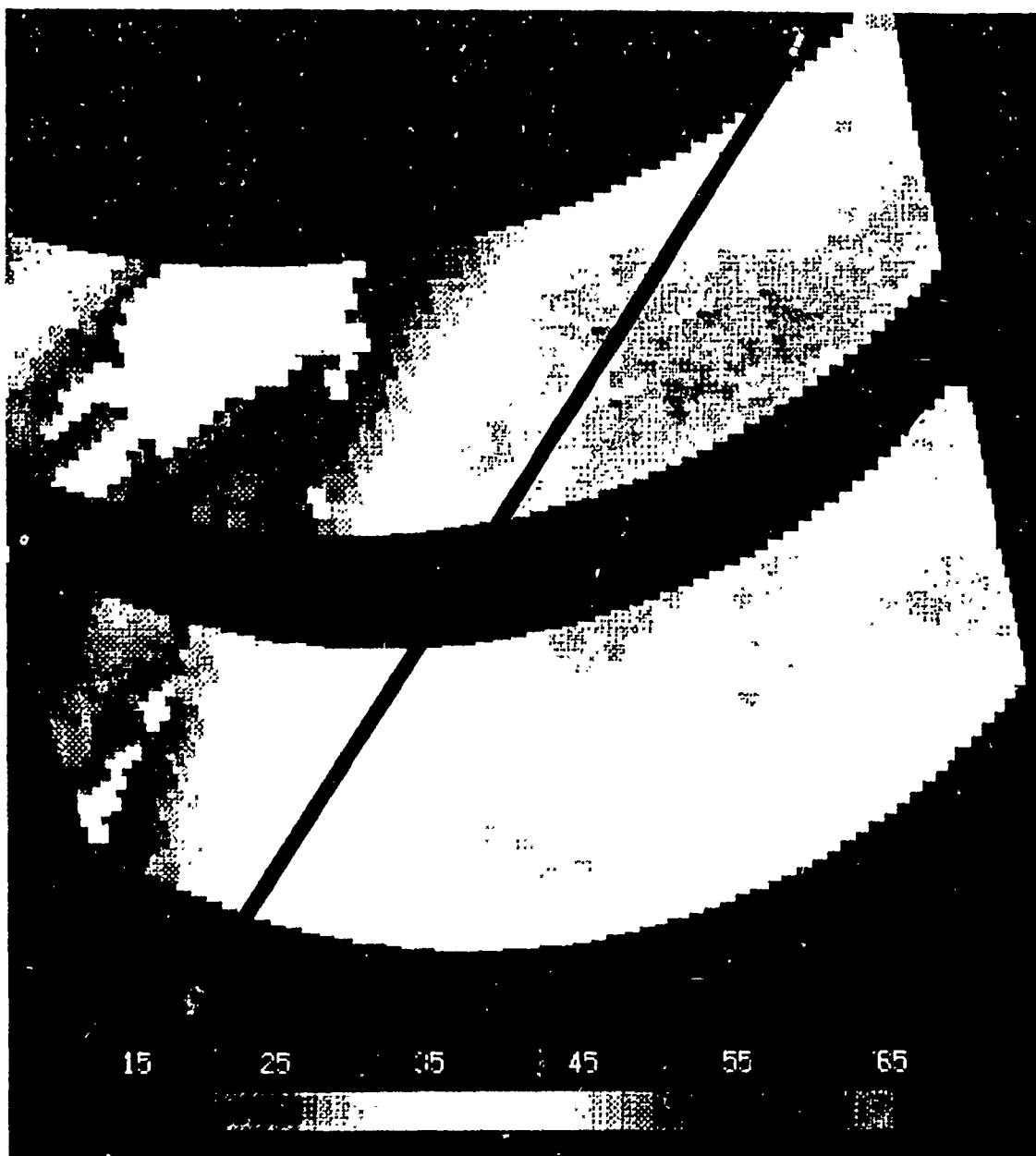


Figure 14 SSM/I water vapor field (kg/m^2); orbit 8934. Line through field represents the GEOSAT flight path.

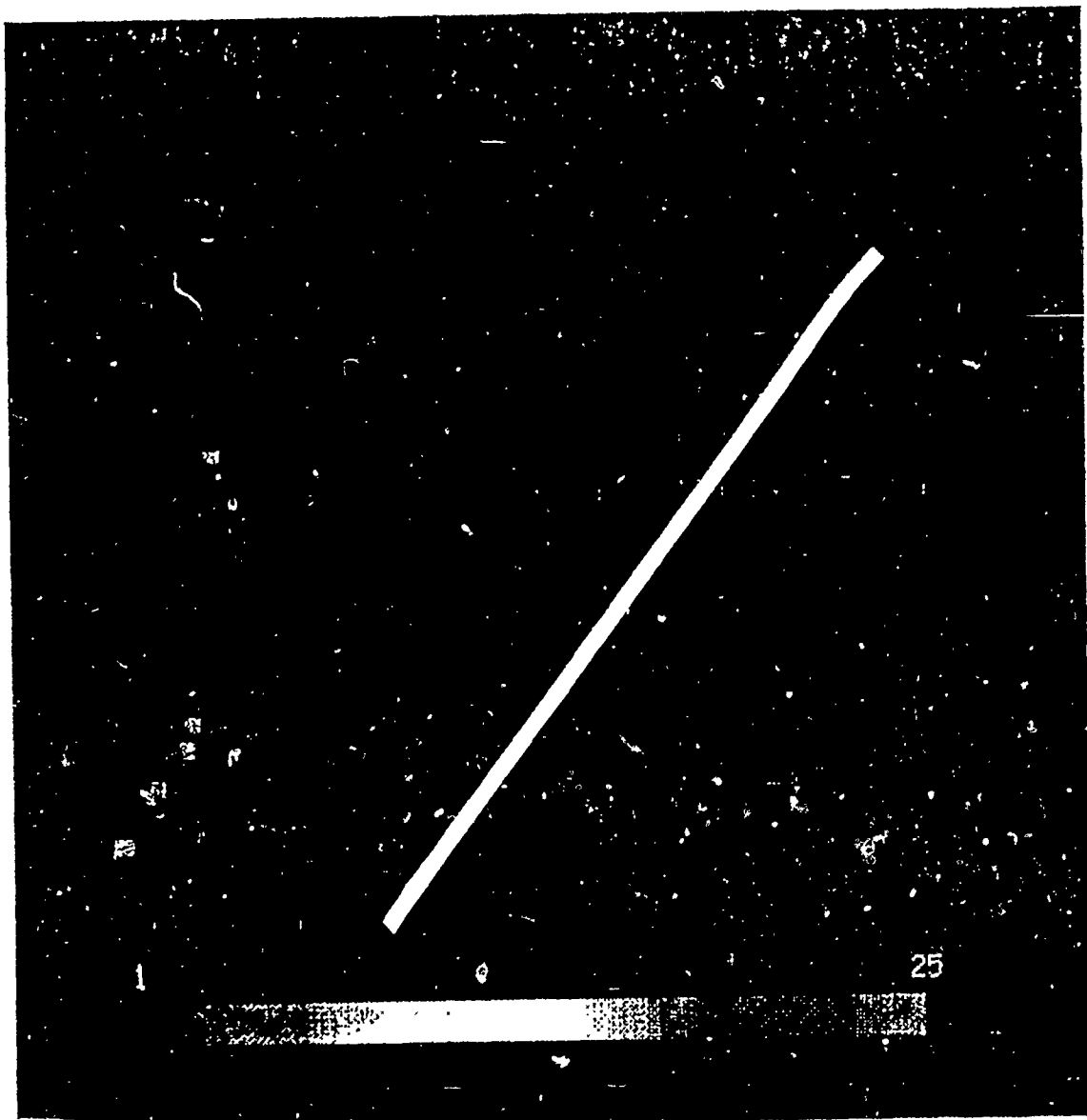


Figure 15 SSM/I precipitation field (mm/hr); orbit 8934. Line through field represents the GEOSAT flight path.

The time difference between the GEOSAT and SSM/I passes is no greater than 1.10 hours. The track of the GEOSAT through the SSM/I swath begins at 49°N, 219°E and altimeter for this particular orbit. By inspection, the correlation between the two instruments is poor. The calculated correlation is 0.208. Fig. 17 illustrates the variation in wind speeds going from latitude 49°N to 57.5°N. Beginning at the most southern point, the difference between the SSM/I and GEOSAT altimeter grow from approximately 1 m/s to as much as 3.5 m/s. The corresponding SSM/I wind field is represented in fig. 18. Examination of the SSM/I water vapor field (Fig. 19), shows the orbit tracks cross a gradient of water vapor which changes from approximately 10 to 30 kg/m² over a distance of about 50 nm. The track continues through an area of saturated water vapor, i.e., greater than 60 kg/m² and then exits into a region of approximately 30 kg/m². The crossing of the gradient at 51°N coincides with the rapid increase in the SSM/I wind speed, while the altimeter remains relatively constant. Examination of the SSM/I precipitation field (Fig. 20) reveals precipitation rates from 1 to 4 mm/hr at 51°N and from 53.5°N to 56°N, along the co-located orbit track. From 56°N to the end of the track, cloud water is present up to 0.125 kg/m² (Fig. 21). This suggests that in regions of cloud water and precipitation, SSM/I winds are greater than GEOSAT values.

SSM/I VS ALTIMETER WIND SPEED

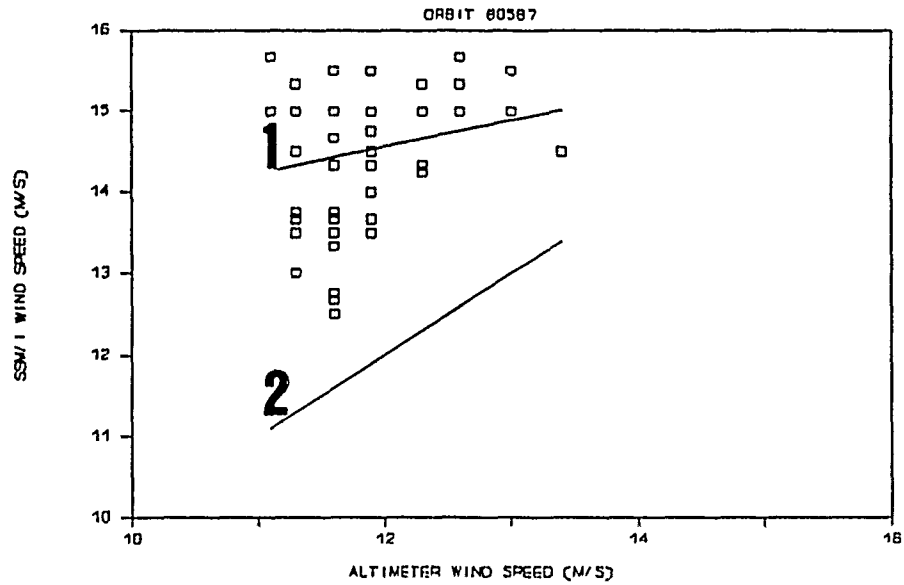


Figure 16 SSM/I vs. GEOSAT wind speed: orbit 80587. Line 1 represents an actual correlation of 0.208, while line 2 represents the reference correlation of 1.0.

WIND SPEED VS. LATITUDE

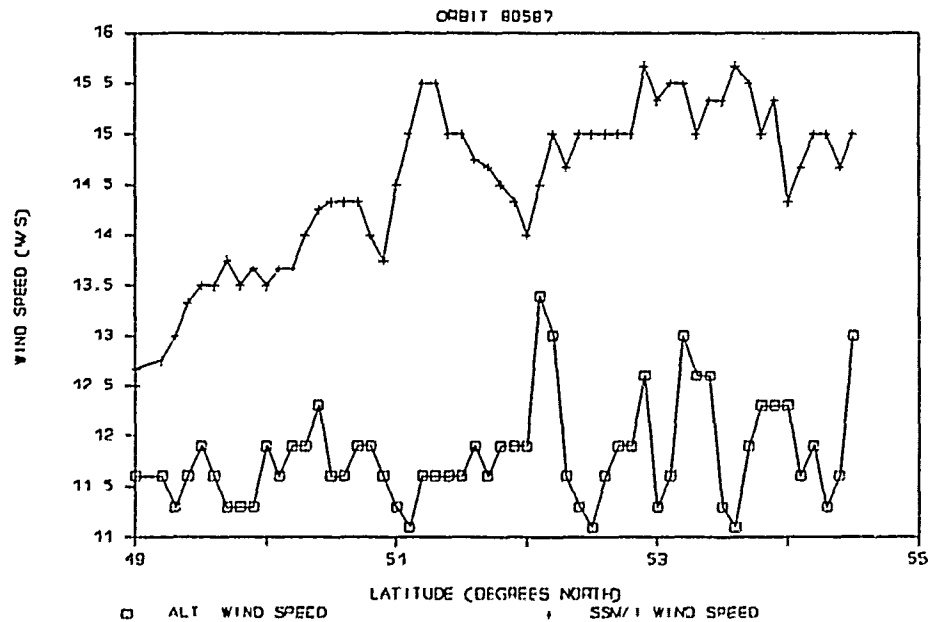


Figure 17 SSM/I and GEOSAT wind speed vs. latitude: orbit 80587.

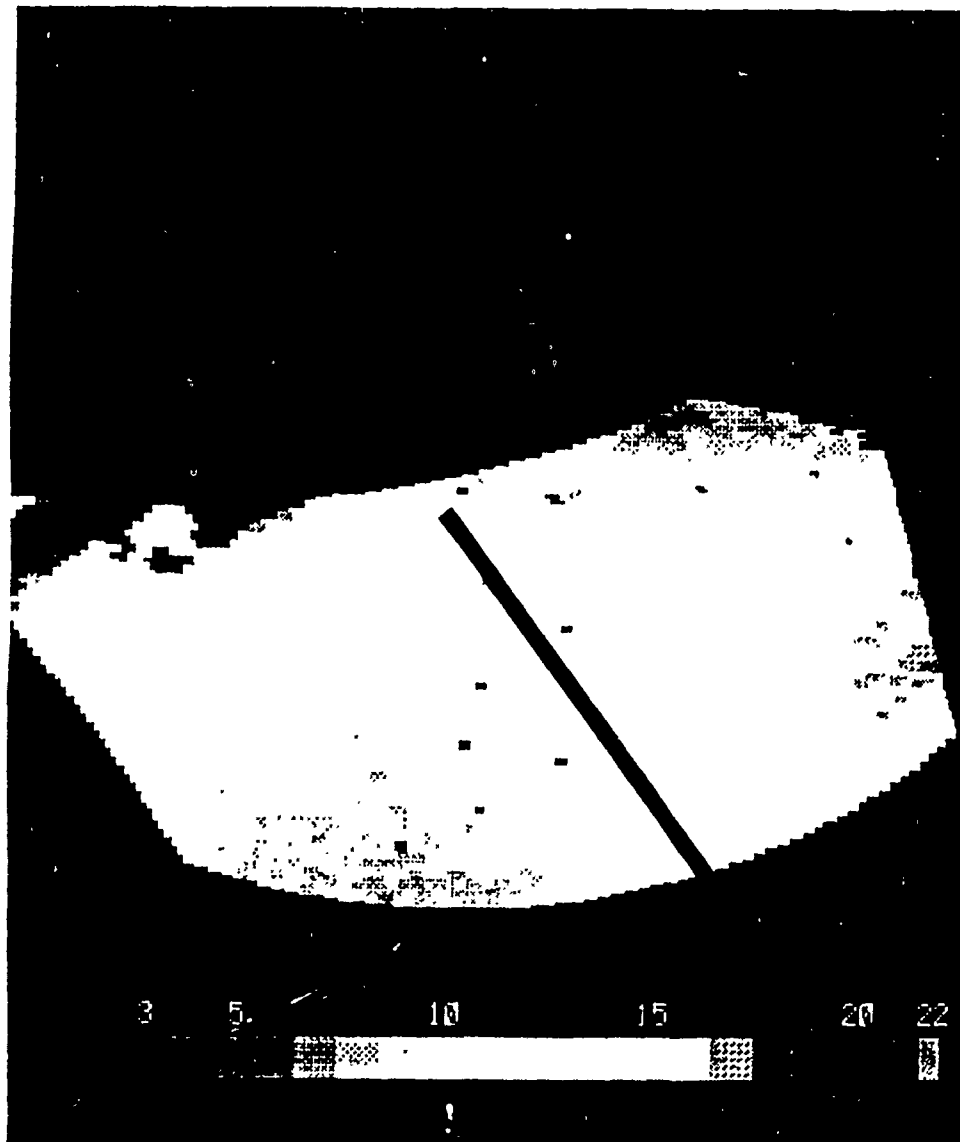


Figure 18 SSM/I wind field (m/s); orbit 8058(7). Line through field represents the GEOSAT flight path.



Figure 19 SSM/I water vapor field (kg/m^2); orbit 8058(7). Line through field represents the GEOSAT flight path.

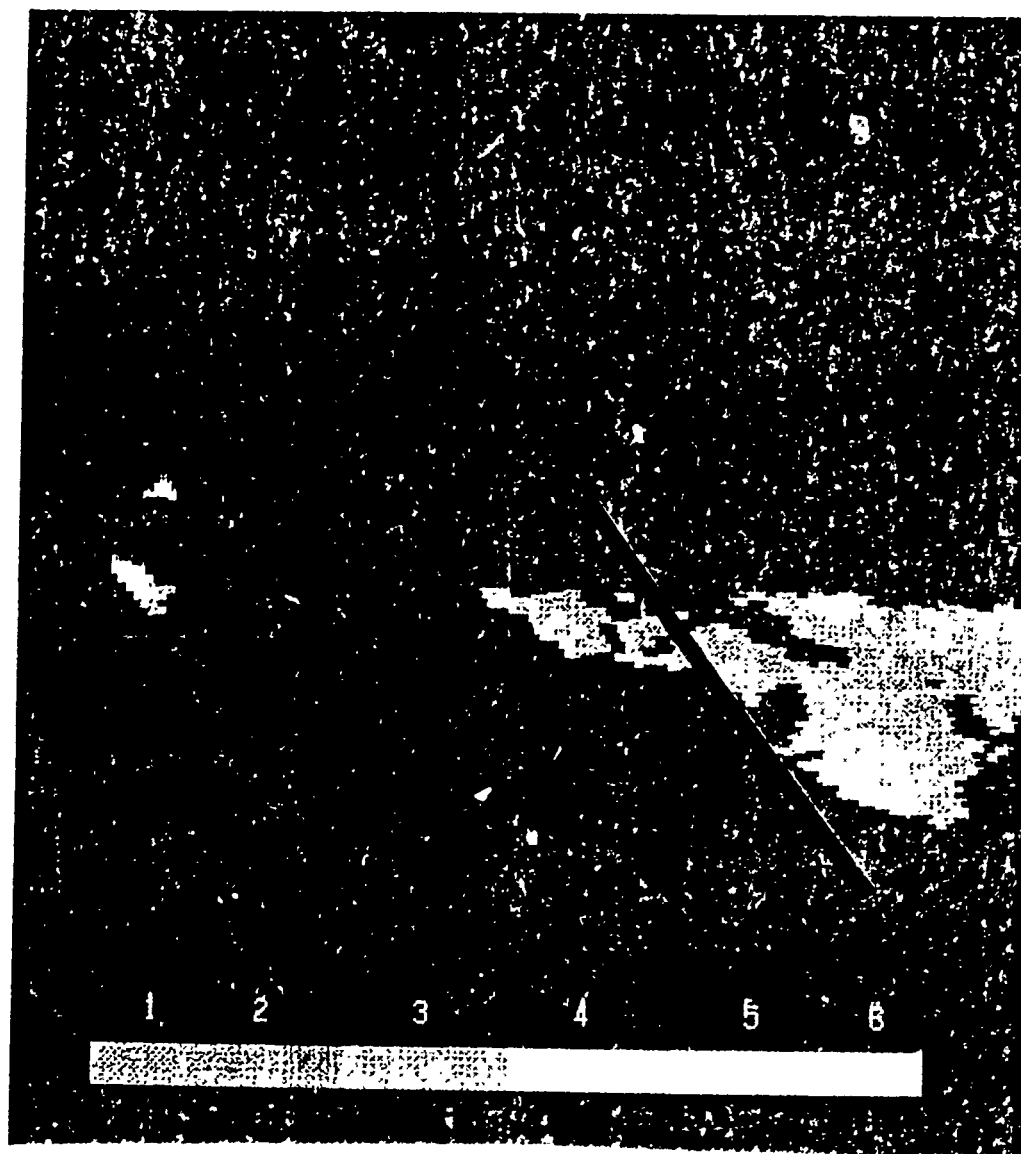


Figure 20 SSM/I precipitation field (mm/hr); orbit 8058(7). Line through wind field represents the GEOSAT flight path.

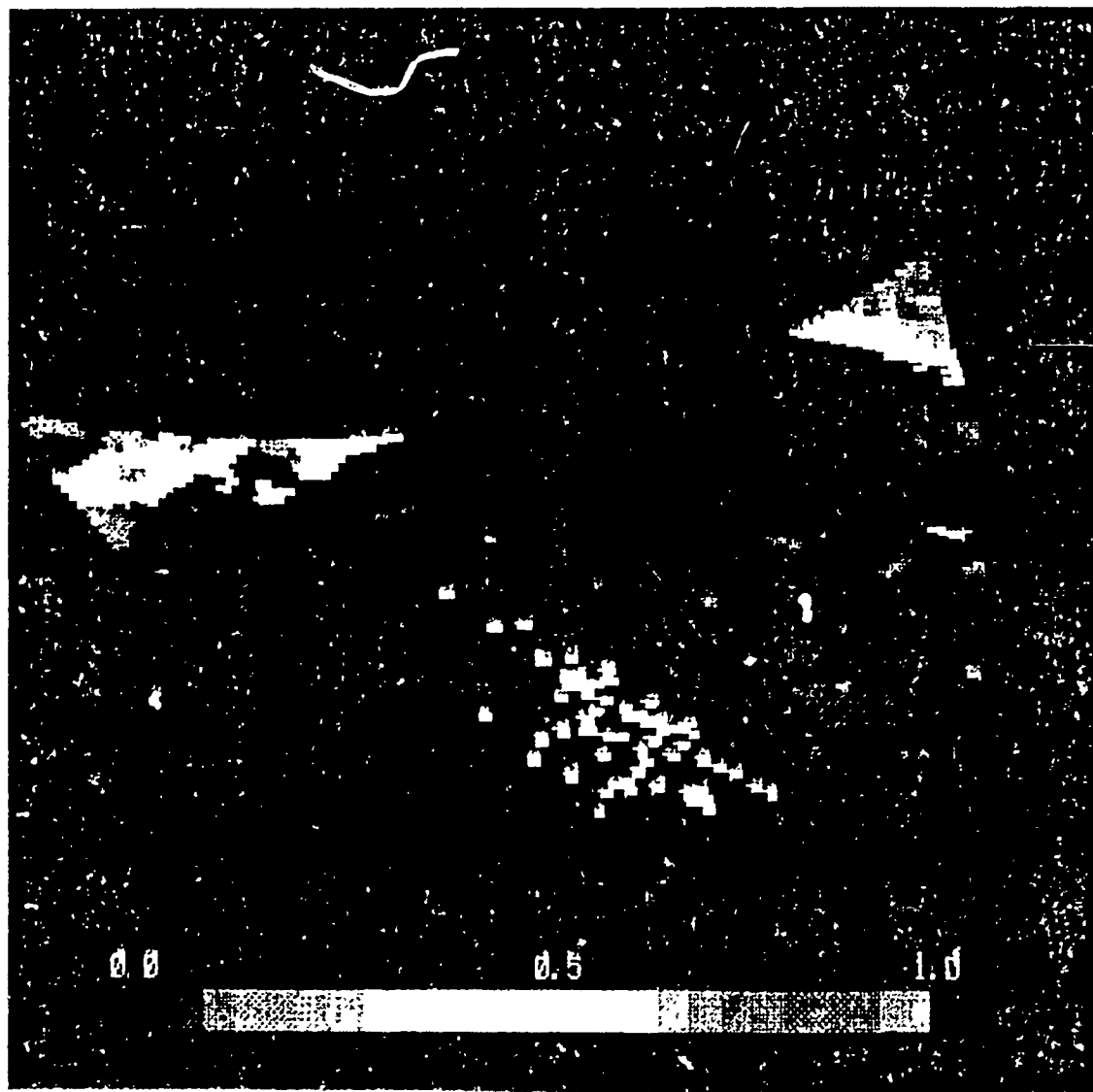


Figure 21 SSM/I cloud water field (kg/m^2); orbit 8058(7). Line through field represents the GEOSAT flight path.

4. Orbit 8058(6), 10 January, 1989

The scan area of the SSM/I encompassed a region bounded by the following coordinates:

<u>Latitude</u>	<u>Longitude</u>
51.88°N	223.64°E
48.89°N	205.01°E
42.14°N	225.01°E
39.60°N	210.11°E

The time difference between the GEOSAT and SSM/I passes is within 1.00 hours. The track of the GEOSAT through the SSM/I swath begins at 40.8°N,224.6°E and ends at 49.5°N,218.6°E. The corresponding graph of SSM/I vs GEOSAT wind fields is presented in Fig. 22. This data set spans a range of wind speeds from 7 to 12 m/s. The correlation in this graph is good below 8 m/s and then the SSM/I appears to read slightly higher than the GEOSAT altimeter. Overall, the correlation is calculated to be 0.935. A graph of wind speed versus latitude (Fig. 23) shows that both instruments were within 1 m/s from 41°N to about 46.5°N and afterwards the difference began to open to about 2 m/s near 48.5°N. Examination of the SSM/I wind field (fig. 24) shows that the location where the difference in wind speed begins to grow occurs around the same area that the wind speeds begin to increase rapidly. The SSM/I water vapor field (Fig. 25) does not demonstrate any significant gradient which would interfere with the measurement of wind speed or any area on increased water vapor.

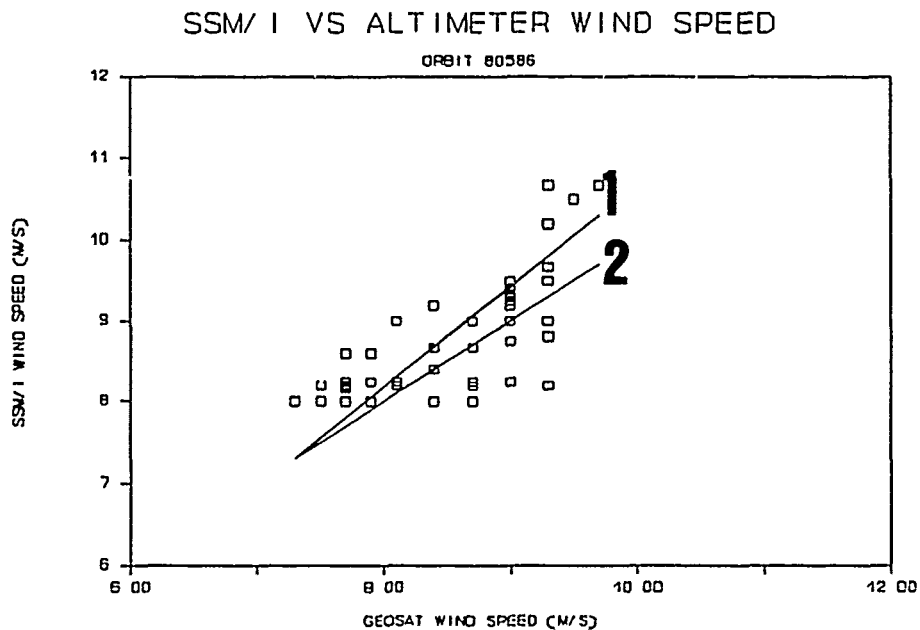


Figure 22 SSM/I vs. GEOSAT wind speed: orbit 80586. Line 1 represents an actual correlation of 0.935, while line 2 represents a reference correlation of 1.0.

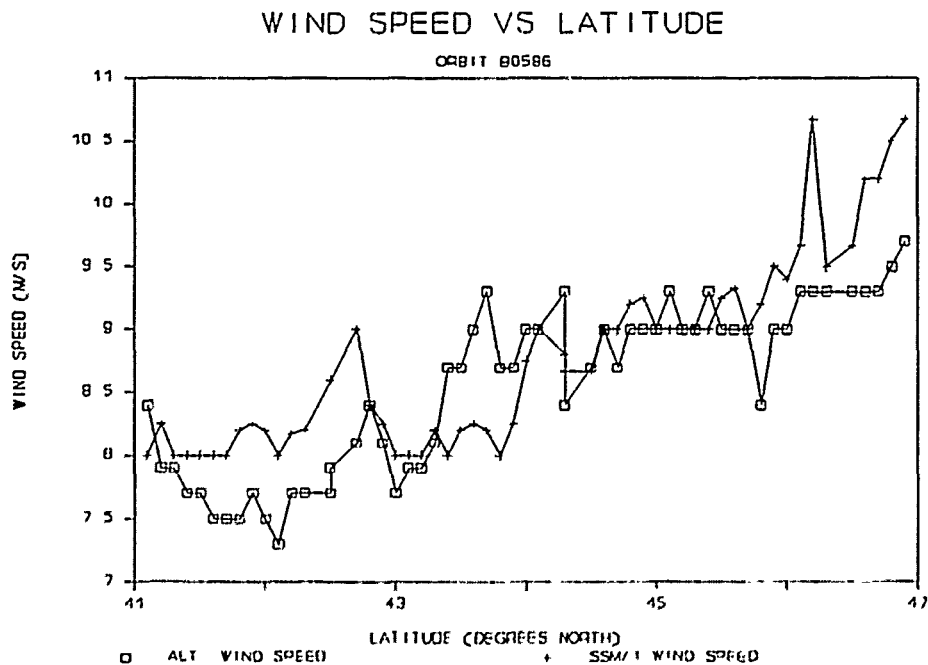


Figure 23 SSM/I vs. GEOSAT winds vs. latitude: orbit 8058(6).

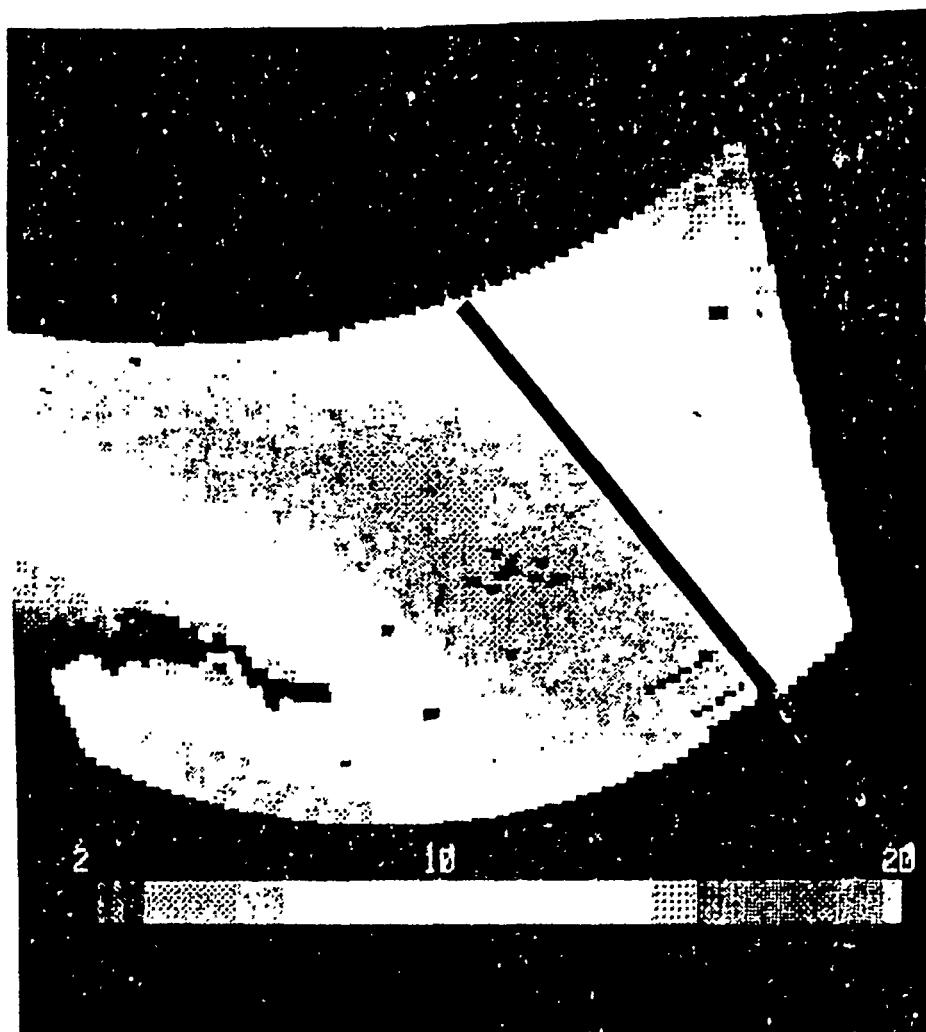


Figure 24 SSM/I wind speed field (m/s): orbit 8058(6). Line represents the GEOSAT flight path.

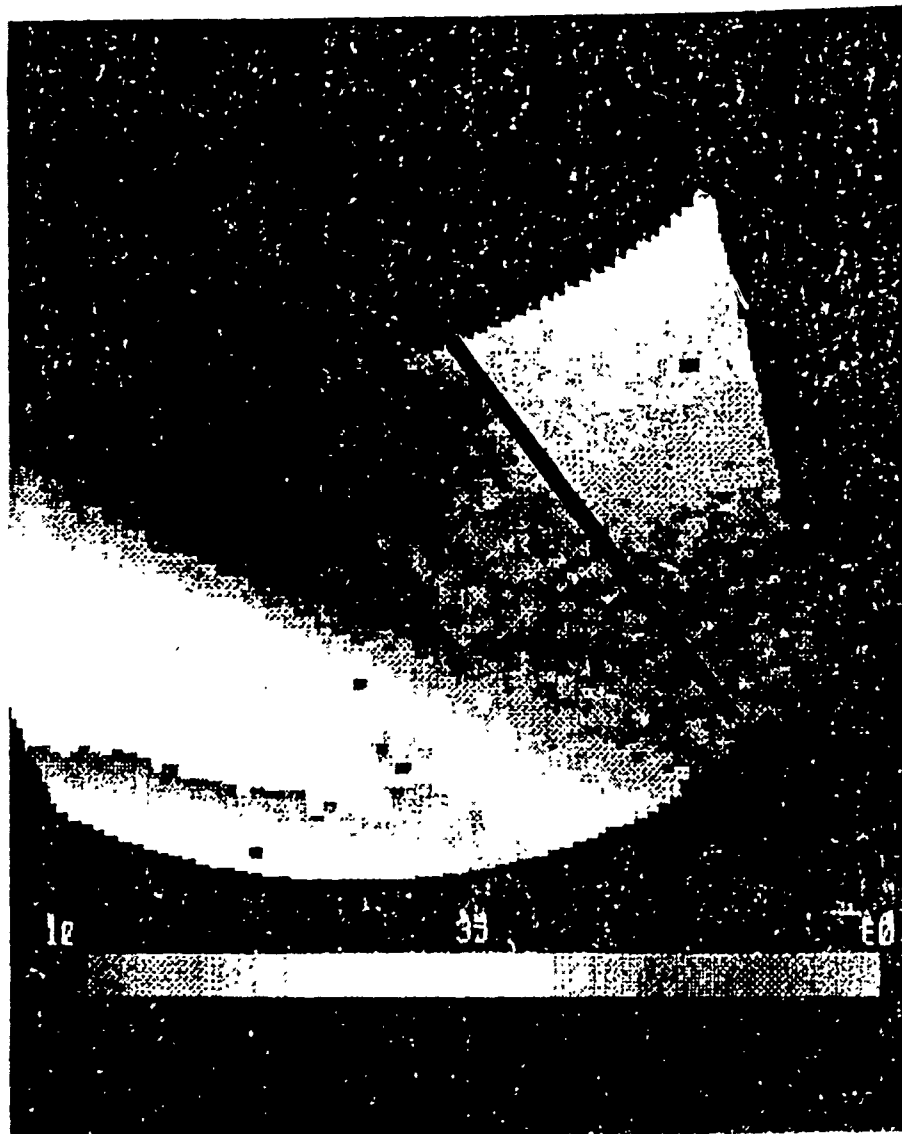


Figure 25 SSM/I water vapor field (kg/m^2): orbit 8058(6). Line through field represents the GEOSAT flight path.

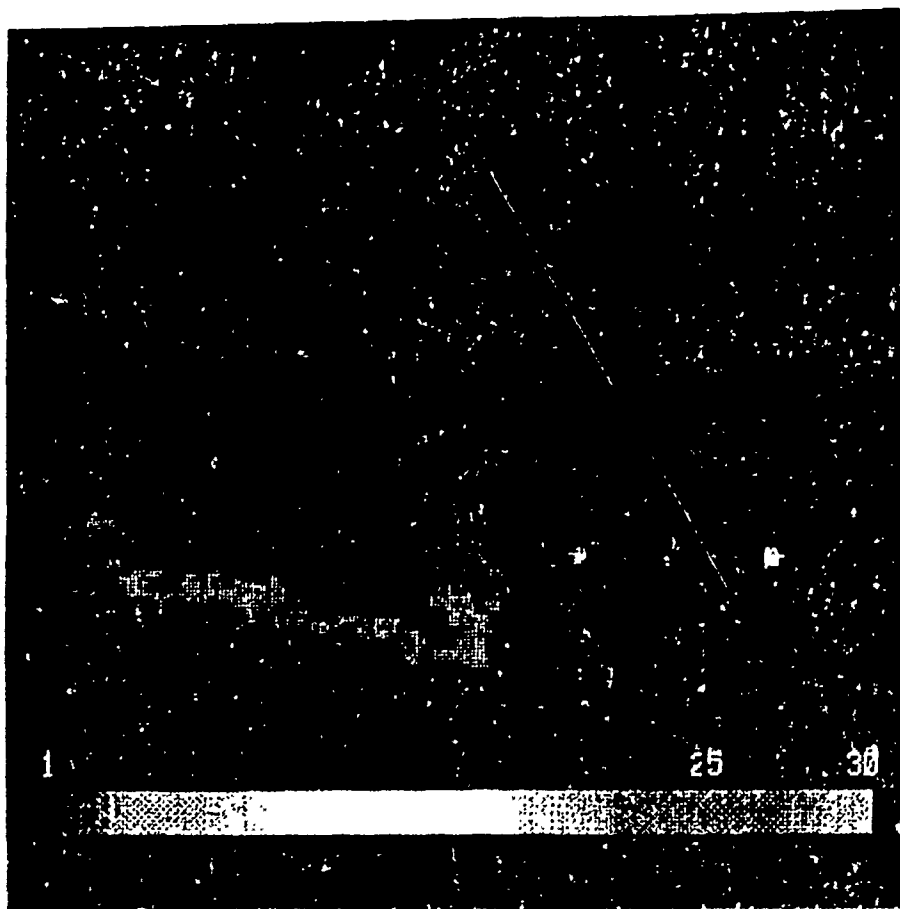


Figure 26 SSM/I precipitation field (mm/hr): orbit 8058(6). The line through the field represents the GEOSAT flight path.

There is, however, a gradual increase in water vapor content in the northeast quadrant of the field from 15 to 30 kg/m². The precipitation field (Fig. 26) shows precipitation to the northeast of the GEOSAT-SSM/I track, but again, there is no evidence of precipitation occurring along the track. Overall, there appeared to be no interfering atmospheric substances in the region of the co-located orbits.

5. Orbit 7925, 2 January, 1989

The scan area of the SSM/I encompassed a region bounded by the following coordinates:

<u>Latitude</u>	<u>Longitude</u>
79.98°N	335.99°E
70.99°N	296.68°E
52.27°N	348.24°E
49.25°N	329.42°E

The time difference between the GEOSAT and SSM/I passes is less than 0.50 hours. The track of the GEOSAT through the SSM/I swath begins at 54.6°N,343°E and terminates at 65.4°N,324.4°E. The plot of SSM/I versus GEOSAT wind speeds (Fig. 27) demonstrates a tremendous amount of scatter in the data. Wind speeds range from 7.5 m/s to 20.5 m/s. The correlation calculated for this data set is -0.301. Looking at the plot of wind speed versus latitude (Fig. 28), one can see that there are two distinct regions where the difference in wind speeds are greater than 3 m/s. This occurs between 57.5°N and 60°N and again from 63.5°N until 65.3°N. The SSM/I wind field (Fig. 29) exhibits a range of wind speeds from 5 to 31 m/s. The highest wind speeds

occur along a band extending from the south central region of the field toward the coast of iceland. High wind speeds are also observed along the coast of greenland. The SSM/I water vapor field (Fig. 30) exhibits a high concentration of water vapor in the southeast quadrant of the SSM/I and GEOSAT orbits. The large white area in the water vapor image represents values higher than 60 kg/m^2 . An examination of the precipitation field (Fig. 31) discloses a major region of precipitation occurring along the track as well. The location of the precipitation coincides with the same area of Fig. 28 that reveals a large difference in wind speed between the SSM/I and GEOSAT altimeter (57.5°N to 60.0°N). The extent of precipitation appears to cover too small a region to be considered the only reason for the disparity between the GEOSAT and SSM/I wind speeds. The SSM/I cloud water field (Fig. 32) shows that this entire region is covered by high cloud water. From this evidence, the cloud water and precipitation together have apparently caused the large difference in wind speed values between the SSM/I and GEOSAT altimeter.

A second area of concern lies between 63.5°N and 65.3°N (Fig. 28). This area is very close to the coast of Greenland, approximately 120 km at its nearest point. The altimeter wind speed measurement steadily increases as it approaches Greenland, while the SSM/I wind speed measurements decrease. This phenomena may be due to the closeness of the land mass and side lobe effects on the SSM/I. Criteria for nearness to land is not clear at this time. Chelton and McCabe [Ref. 18] and Wentz et al [Ref. 19] consider only those regions where microwave remote sensing is done

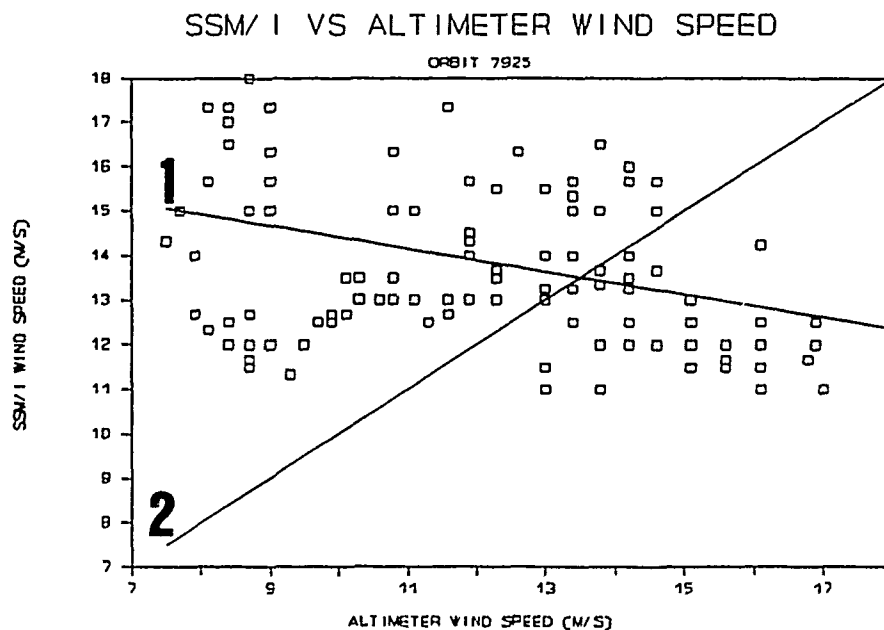


Figure 27 SSM/I vs. GEOSAT wind speed: orbit 7925. Line 1 represents an actual correlation of -0.301, while line 2 represents a reference correlation of 1.0.

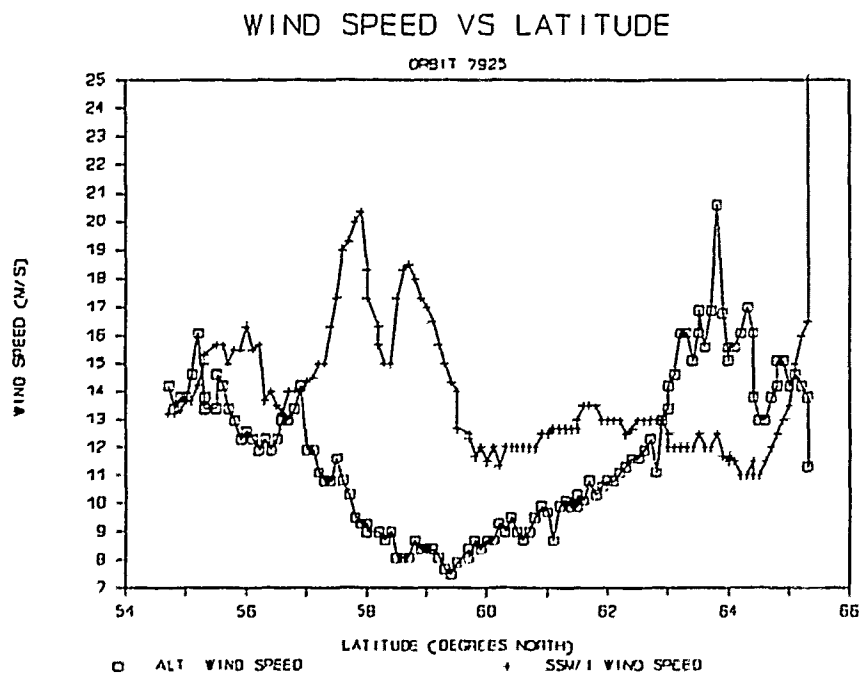


Figure 28 SSM/I and GEOSAT wind speeds vs. latitude.

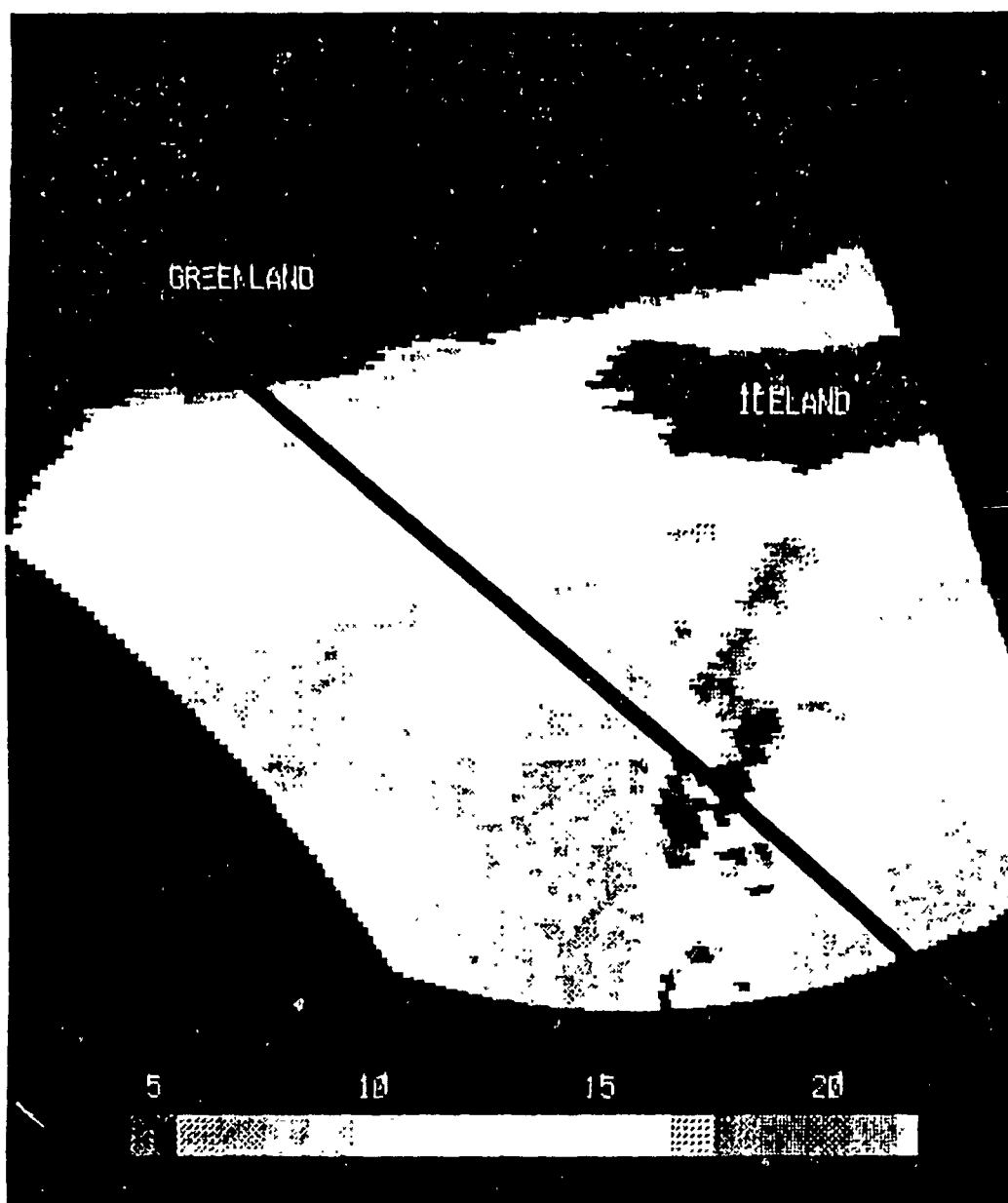


Figure 29 SSM/I wind speed field (m/s); orbit 7925. Line represents the GEOSAT flight path.

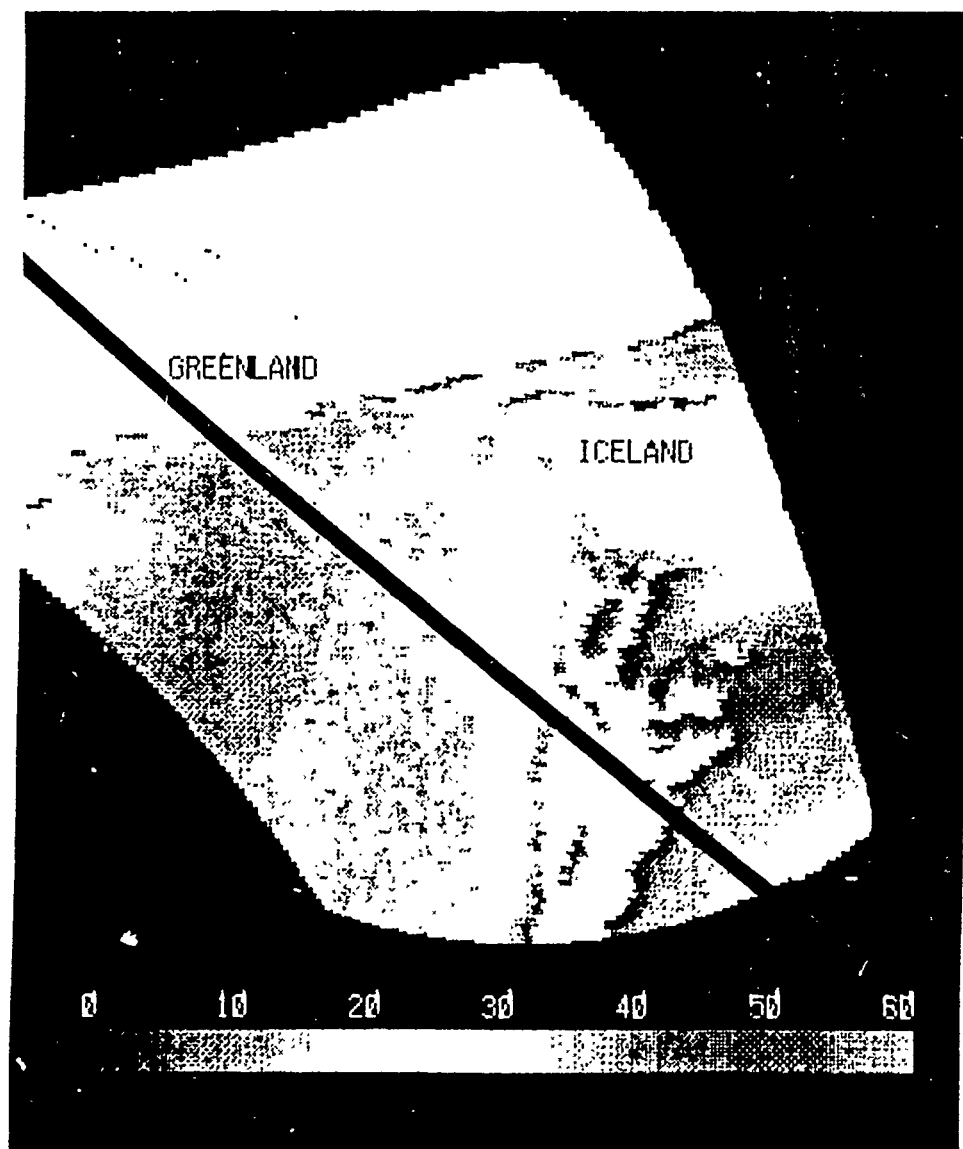


Figure 30 SSM/I water vapor field (kg/m^2); orbit 7925. Line through field represents the GEOSAT flight path.

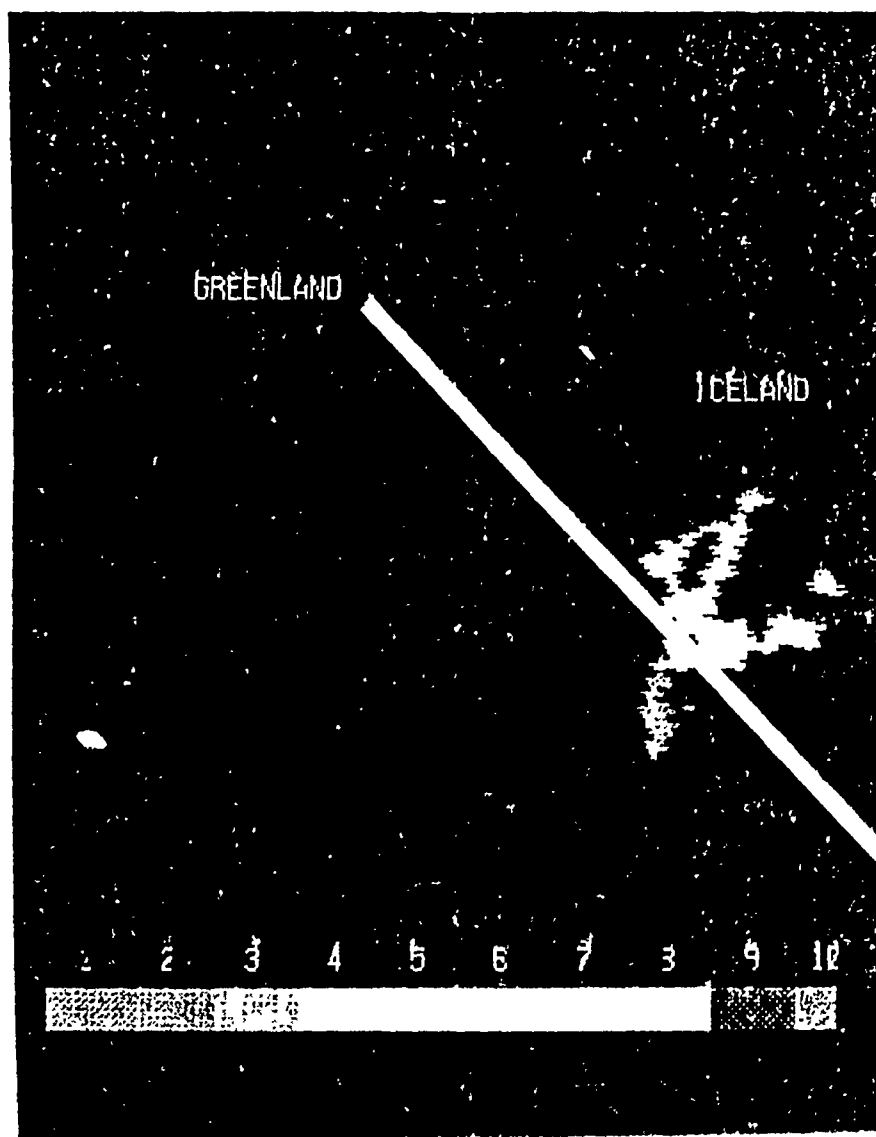


Figure 31 SSM/I precipitation field (mm/hr); orbit 7925. Line through field represents GEOSAT flight path.

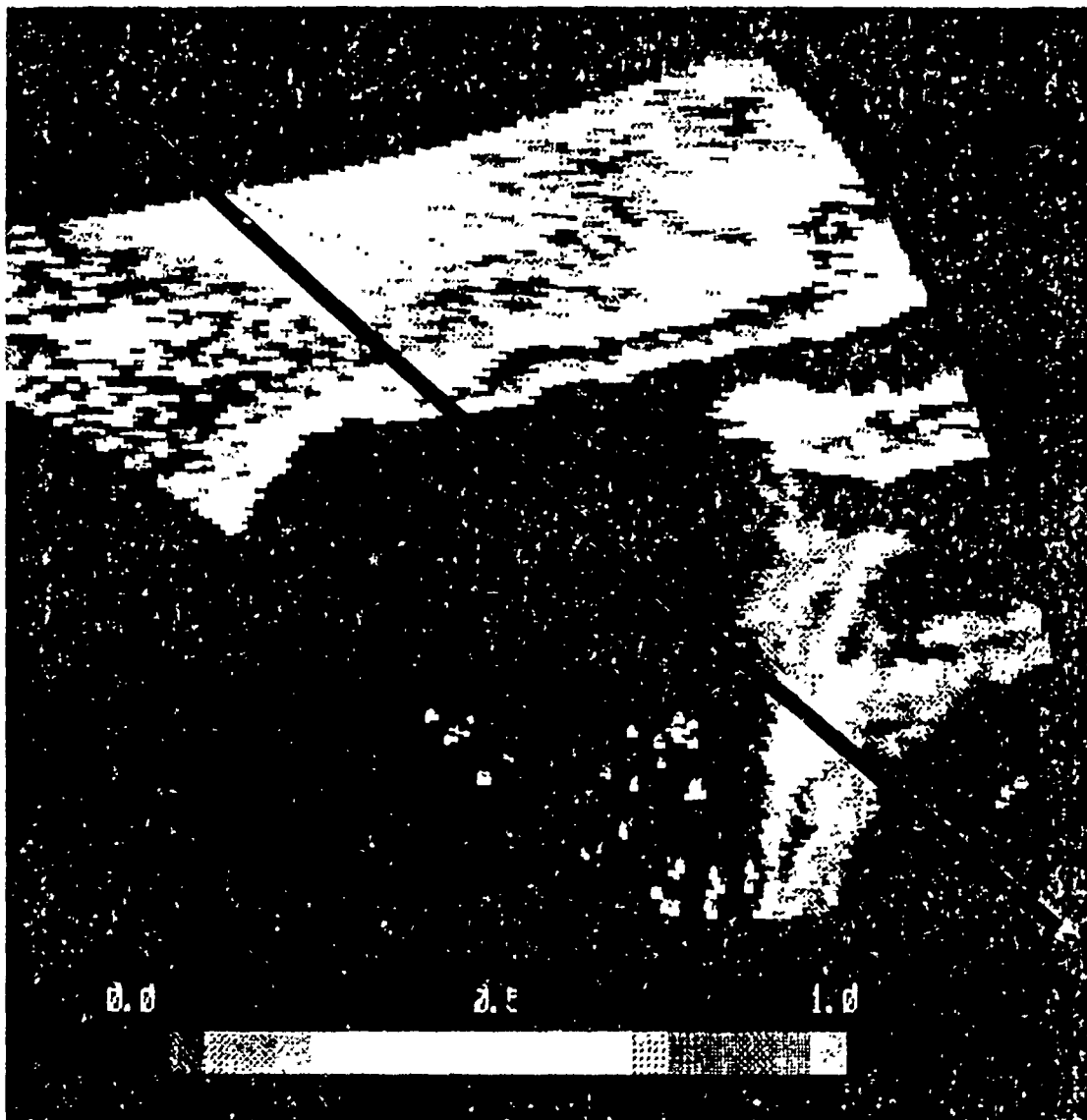


Figure 32 SSM/I cloud water field (kg/m^2); orbit 7925. Line through field represents the GEOSAT flight path.

from 200 to 800 km from the nearest land mass. They sight erratic behavior due to side lobes and the change in emissivity, when making microwave measurements of the open ocean are made close to land.

VII. CONCLUSIONS

To assess the relationship between the wind speeds as measured by the GEOSAT altimeter and the SSM/I, the correlation (R), R^2 , slope and intercept were calculated. Table one contains the results of the analysis of each data set.

The value of R^2 represents the proportion of total variance in the values of the SSM/I wind speed data that can be accounted for by a linear relationship to the GEOSAT wind speeds. In orbits 9138 and 8058(6), more than 90% of the variance is explained by this linear relationship. Orbits 7925 and 8058(7) demonstrate almost no correlation between the SSM/I and altimeter wind speeds.

The intercept gives the bias between wind speed measurements. Orbit 9138 and 8058(6) exhibit the smallest bias, approximately 1 m/s. The accuracy goal of

Table 1. Each data set is identified by its orbit number along with its associated correlation (R), R^2 , intercept, slope, and atmospheric parameters present during the wind speed measurement.

<u>ORBIT</u>	<u>R</u>	<u>R²</u>	<u>SLOPE</u>	<u>INTERCEPT</u>	<u>COMMENTS</u>
9138	0.925	0.8583	1.284	-1.297	High water vapor concentration
8934	0.616	0.5070	0.644	6.889	Clear Atmosphere
8058(7)	0.208	0.0431	0.329	10.599	Precipitation, cloud water, and water vapor
8058(6)	0.935	0.8739	1.247	-1.800	Clear Atmosphere
7925	0.301	0.0900	0.258	16.980	Precipitation, cloud water, and water vapor

the GEOSAT altimeter and the SSM/I has been 2 m/s. Both orbits 9138 and 8058(6) are within that goal. Orbits 7925, 8058(7), and 8934 have a bias in wind speed greater than 2 m/s. The slope is also a good indicator of the relationship between the SSM/I and GEOSAT altimeter wind speeds. A perfect relationship between wind speed measurements would give a slope of 1.0. Orbits 9138 and 8058(6) have a slope very close to one, while 7925 and 8058(7) have a slope near 0.0.

There are four conclusions that are made from the analysed data in this paper:

(1) The data sets which did not contain cloud water or precipitation along the co-located SSM/I and GEOSAT orbits (orbits 9138, 8934, and 8058(6)), demonstrated a good correlation between the two systems.

(2) Although a large amount of water vapor was present along the entire track of orbit 9138, there appeared to be no evidence of bias with the measured wind speeds from either instrument. Since the SSM/I corrects for the presence of water vapor in the atmosphere, it is obvious, from the high correlation between the GEOSAT altimeter and the SSM/I, that the SSM/I water vapor correction works well. The altimeter was not corrected for water vapor, suggesting that water vapor corrections on the altimeter were small.

(3) The data sets which contained cloud water and precipitation (orbits 8058(7) and 7925), displayed large differences in recorded wind speeds between the SSM/I and GEOSAT altimeter. In these areas, the SSM/I wind speed would increase, while the altimeter wind speed decreased relative to one another and, consequently, very poor correlation resulted. There are several explanations for the difference in

wind speed relative to each other experienced by both sensors. The increased emissivity associated with precipitation, or cloud water, is the most likely cause of increased wind speeds experienced by the SSM/I, by introducing a "warm " atmospheric term. The GEOSAT may experience a decrease in wind speed at the same location. This may have been a result of a decrease in ocean surface roughness. The reduction in surface roughness is caused by rain drops impacting on the ocean surface and consequently attenuating the surface gravity waves [Ref. 21] . The reduction in surface roughness would result in a larger backscatter cross section for the GEOSAT altimeter. This reduced backscatter is interpreted as a decrease in wind speed, which is what is observed in the area of precipitation in orbits 7925 and 8058(7). An alternative explanation for the low GEOSAT wind speed in the area of precipitation is that the measurement was correct and that the SSM/I had a bias to high wind speeds in the presence of rain.

(4) Erratic behavior is seen in microwave measurements of the open ocean near a land mass. This is evident in orbit 7925 when measurements of wind speed and atmospheric properties were made within 120 km of the Greenland coastline. The resulting data from the coastal areas was highly erratic. Based on only one data set near a coastal feature, it appears that wind speed measured within 200 km of a land mass is not reliable. This is most likely due to the radiance detected by antenna sidelobes which mask the actual measurement of radiation from the main lobe of the antenna.

The wind speed verification studies of the GEOSAT altimeter and the SSM/I demonstrate that both active and passive microwave systems measure similar values

of wind speed over the ocean. These instruments are comparable in open ocean regions at least 200 km from land and free of cloud water and precipitation. Utilization of GEOSAT altimeter and SSM/I wind speed data in a numerical forecasting model requires that a system for screening wind data for cloud water, precipitation, and proximity to land masses be used.

LIST OF REFERENCES

1. Stewart, R.H., Methods of Remote Sensing, pp.28-44, University of California Press, 1985.
2. Elachi, C., Introduction to the Physics and Techniques of Remote Sensing, pp.25-26, 1987.
3. Schanda, E., Remote Sensing For Environmental Sciences, Berlin: Springer-Verlag, pp.367, 1976.
4. Lane, J.A. and Saxton, J.A., "Dielectric Dispersion in Pure Polar Liquids at Very High Radio Frequencies", Proceedings of the Royal Society of London, 214A, pp.531-545, 16 May 1952.
5. Businger, J.A., "Turbulent Transfer in the Atmospheric Surface Layer", Workshop on Micrometeorology, pp.67-81, 1979.
6. Stull, R.B., "An Introduction to Boundary Layer Meteorology", Kluwer Academic Publishers, pp.377-386, 1988.
7. Hollinger, J., Lo, R., Poe, G., Savage, R., Pierce, J., "Special Sensor Microwave Imager User's Guide", Naval Research Laboratory, pp.A23-A24, 14 September 1987.
8. Swift, C.T., "Passive Microwave Remote Sensing of the Ocean; A Review", Boundary Layer Meteorology, v.18, pp.25-54, 1980.
5. Wilheit, T.T., "The Effect of Wind on the Microwave Emission from the Ocean's Surface at 37 GHz", Journal of Geophysical Research, v.84, pp.4921-4926, 20 August 1979.
10. Hollinger, J., Lo, R., Poe, G., Savage, R., Pierce, J., "Special Sensor Microwave Imager User's Guide", Naval Research Laboratory, p.A24, 14 September 1987.
11. McConathy, D.R., Kilgus, C.C., "The Navy GEOSAT Mission: An Overview", Johns Hopkins APL Technical Digest, v.8, pp.170-175, April-June 1987.
12. MacArthur, J.L., Marth, P.C., Wall, J.G., "The GEOSAT Radar Altimeter", Johns Hopkins APL Technical Digest, v.8, pp.176-181, April-June 1987.
13. Mognard, N., Lago, B., "The Computation of Wind Speed and Wave Heights from GEOS 3 Data", Journal of Geophysical Research, V.84, pp.3979-3986, 3 January 1979.

14. Cox, C., Munk, W., "Some Problems in Optical Oceanography", Journal of Marine Research, v.14, pp.63-78, 1955.
15. Cox, C. and Munk, W., " The Measurement of the Roughness of the Sea Surface From Photographs of the Sun's Glitter", Journal of the Optical Society of America, v.44, pp.838-850, 1954.
16. Brown, G.S., "Estimation of Surface Wind Speeds Using Satellite-Borne Radar Measurements at Normal Incidence", Journal of Geophysical Research, v.84, pp.3974-3978, 30 July 1979.
17. Shuhy, J.L., Grunes, M.R., Uliana, E.A., Choy, L.W., "Comparison of GEOSAT and Ground Truth Wind and WAVE Observations: Preliminary Results", Johns Hopkins APL Technical Digest, v.8, pp.219-221, April-June 1987.
18. Hollinger, J.P., Poe, G.A., "DMSP SSM/I CAL/VAL Interim Report", Naval Research Laboratory, 1988.
19. Chelton, D.B. and McCabe, P.J., " Satellite Altimeter Measurement of Sea Surface Wind Speed", Journal of Geophysical Research, v.80, pp.4707-4720, 20 May 1985.
20. Wentz, F.J. and Mattox, L.A., " New Algorithms for Microwave Measurements of Ocean Winds: Applications to SEASAT and the Special Sensor Microwave Imager", Journal of Geophysical Research, v. 91, pp.2289-2307, 15 February 1986.
21. Nystuen, J.A., "A Note On The Attenuation of Surface Gravity Waves by Rainfall", submitted to the Journal of Geophysical Research, August 1989.

INITIAL DISTRIBUTION LIST

- | | | |
|----|--------------------------------------|---|
| 1. | Defense Technical Information Center | 2 |
| | Cameron Station | |
| | Alexandria, Virginia 22304-6145 | |
| 2. | Library, Code 0142 | 2 |
| | Naval Postgraduate School | |
| | Monterey, California 93943-5002 | |
| 3. | Chairman (Code 63Rd) | 1 |
| | Department of Meteorology | |
| | Naval Postgraduate School | |
| | Monterey, California 93943-5000 | |
| 4. | Chairman (Code 68Co) | 1 |
| | Department of Oceanography | |
| | Naval Postgraduate School | |
| | Monterey, California 93943-5000 | |

- | | | |
|----|--|---|
| 5. | Professor Jeffrey A. Nystuen(Code 68Ny) | 5 |
| | Department of Oceanography | |
| | Naval Postgraduate School | |
| | Monterey, California 93943-5000 | |
| 6. | Dr. Andreas K. Goroch | 1 |
| | Naval Environmental Prediction and Research Facility | |
| | Monterey, California 93943 | |
| 7. | LT. James E. Lilly, USN | 2 |
| | 1418 Robinwood Drive | |
| | Milton, Florida 32570 | |
| 8. | Director Naval Oceanography Division | 1 |
| | Naval Observatory | |
| | 34th and Massachusetts Avenue NW | |
| | Washington DC 20390 | |
| 9. | Commander Naval Oceanography Command | 1 |
| | Stennis Space Center, Mississippi 39529-5000 | |

- | | | |
|-----|--|---|
| 10. | Commanding Officer | 1 |
| | Naval Oceanographic Office | |
| | Stennis Space Center, Mississippi 39522-5001 | |
| | | |
| 11. | Commanding Officer | 1 |
| | Fleet Numerical Oceanography Center | |
| | Monterey, California 93943 | |
| | | |
| 12. | Commanding Officer | 1 |
| | Naval Ocean Research and Development Activity | |
| | Stennis Space Center, Mississippi 39522-5001 | |
| | | |
| 13. | Commanding Officer | 1 |
| | Naval Environmental Prediction Research Facility | |
| | Monterey, California 93943 | |
| | | |
| 14. | Chairman, Oceanography Department | 1 |
| | U.S. Naval Academy | |
| | Annapolis, MD 21402 | |

15. Chief of Naval Research 1
800 North Quincy Street
Arlington, Virginia 22217
16. Office of Naval Research (Code 420) 1
Naval Ocean Research and Development Activity
800 North Quincy Street
Arlington, Virginia 22217
17. Scientific Liason Office 1
Office of Naval Research
Scripps Institution of Oceanography
La Jolla, California 92037
18. Library 1
Scripps Institution of Oceanography
P.O. Box 2367
La Jolla, California 92037
19. Library 1
Department of Oceanography
University of Washington
Seattle, Washington 98105